Journal of Computational Physics 366 (2018) 144–169

Contents lists available at ScienceDirect

Journal of Computational Physics

www.elsevier.com/locate/jcp

# A unified gas-kinetic scheme for axisymmetric flow in all Knudsen number regimes

Shiyi Li [a], Qibing Li [a,*], Song Fu [a], Kun Xu [b]

[a] AML, Department of Engineering Mechanics, Tsinghua University, Beijing 100084, China
[b] Department of Mathematics, Hong Kong University of Science and Technology, Clear Water Bay, Hong Kong, China

ARTICLE INFO

*Article history:*
Received 10 September 2017
Received in revised form 21 March 2018
Accepted 2 April 2018
Available online 5 April 2018

*Keywords:*
UGKS
Axisymmetric flow
Source term
Multiscale
Implicit scheme

ABSTRACT

Based on kinetic model equation, a unified gas-kinetic scheme for axisymmetric flow (UGKS-AS) is proposed in the whole flow regimes. The flux transport of UGKS-AS is based on a reduced gas distribution function of a time integral solution of the full 3D BGK model. In the cylindrical coordinate system, the local time evolution of convection and source terms for the macroscopic and microscopic flow variables is fully coupled with particle free transport and collisions. As a result, a multiple scale UGKS-AS is developed and used for the flow simulation from the free molecular transport to the Navier–Stokes solutions. In comparison with the full 3D UGKS method for axisymmetric flow, the present scheme is much more efficient and gives accurate solution in all flow regimes. Different from operator splitting methods with decoupled treatment of particle transport and collision, for the Navier–Stokes solution in the continuum regime the UGKS-AS doesn't have the constraint on the time step being less than the particle collision time. To further improve the efficiency of the scheme for steady state solution, an implicit UGKS-AS method is also developed. A large number of numerical tests for axisymmetric flow are conducted by the proposed explicit and implicit UGKS-AS, which include inner and outer, steady and unsteady, low and high speed flows. Some tests are very challenging due to the delicate capturing of very small flow variations. The good agreement among the solutions from the present scheme and other analytical, numerical, and experimental studies, validates the high accuracy and efficiency of the UGKS-AS for non-equilibrium flow simulation in all regimes.



## 1. Introduction

Axisymmetric flows in all flow regimes occur in nature and have wide engineering applications. Instead of solving the full three-dimensional (3D) kinetic model equation for axisymmetric flow, it is no doubt much cheaper to construct a scheme based on the quasi two-dimensional (2D) axisymmetric model equation, without the discretization in the circumferential direction [1,2]. Furthermore the axial symmetry of the flow can be better preserved when using quasi 2D axisymmetric model in the numerical simulation. In addition, the quasi-2D axisymmetric computation can avoid the cumbersome mesh generation and singularity near the symmetric axis. Although it can also be achieved using unstructured meshes in the 3D

* Corresponding author.
*E-mail addresses:* shiyi-li12@mails.tsinghua.edu.cn (S. Li), lqb@tsinghua.edu.cn (Q.B. Li), fs-dem@tsinghua.edu.cn (S. Fu), makxu@ust.hk (K. Xu).

https://doi.org/10.1016/j.jcp.2018.04.004
0021-9991/

computation [3,4], the quasi-2D axisymmetric simulation is superior in computational cost and axial symmetry preserving when solving axisymmetric flows.

Many quasi-2D models and schemes for axisymmetric flow have been developed in the previous studies [1,2,5–9]. Most of them are based on Bhatnagar–Gross–Krook (BGK) type kinetic equations. It is much more difficult to construct a delicate scheme for quasi-2D axisymmetric model equations than those schemes for 2D and 3D models in a purely Cartesian coordinate system.

In cylindrical coordinate the kinetic equation includes geometric source term. A consistent discretization of the velocity derivative of the source term is important for improving the quality of the scheme in terms of resolution, robustness, and conservation. Assiduous work has been done to seek for an efficient algorithm to approximate the velocity derivative [1, 10]. Mieussens [1] systematically studied the accuracy and conservation of several approaches for the velocity derivative operators and also proposed trigonometric operators with good efficiency when applied in some typical axisymmetric flows. On the other hand, many researches are searching for appropriate simplification of the axisymmetric source term. One of the models is based on the assumption of Maxwellian distribution in the circumferential direction and non-equilibrium states in the axial and radial directions, which is partly supported by numerical observation [11]. Consequently, the highly nonlinear source term in a quasi-2D model is simplified to be a linear one which can be easily approximated with coarse velocity mesh points in the discrete velocity method (DVM) [6]. The distribution function in the source term has been further approximated by the Chapman–Enskog expansion and a lattice Boltzmann method for low-speed axisymmetric flows has been constructed [2,12]. However, these simplifications are restricted for flow simulation close to continuum regime. In fact, with the help of the Chapman–Enskog expansion in the construction of the initial distribution function and the time evolution of the equilibrium state, the Gas-Kinetic Scheme (GKS) based on the integral solution of BGK equation has been developed [13] and extended to the axisymmetric flow computation for the Navier–Stokes solutions [7,14]. In the continuum flow regime no discretization of the velocity derivatives is required and the scheme works efficiently for the viscous and heat conducting flows.

Recently, based on the analytical solution of BGK type equation, a multiscale unified gas-kinetic scheme (UGKS) has been developed for flow simulation in the whole regimes [15–17,3]. The coupled treatment of the particle free transport and collision for the flux evaluation in UGKS releases the constraint of time step being less than particle collision time and the cell size being less than the particle mean free path, which are suffered by most kinetic equation solvers, including the direct simulation Monte Carlo (DSMC) method.

The UGKS works accurately and efficiently in the whole flow regime and is proved to be able to asymptotically obtain the Navier–Stokes (NS) solutions in continuum flow regime, which is still a challenge for many other kinetic methods [18–20]. To further improve the efficiency of UGKS for steady state computation, the implicit UGKS has been developed [21,22]. However, the existing explicit and implicit UGKS are only for flow computation in Cartesian coordinate with plane geometry. For axisymmetric flow, a new UGKS in cylindrical coordinate is preferred in terms of efficiency and memory reduction. On the other hand, most existing kinetic schemes for axisymmetric quasi-2D models use operator splitting approaches, which decouple the convection term, the axisymmetric source term, and the collision term. It is virtually questionable for these schemes whether they have the property of recovering NS solutions asymptotically in the continuum flow regime.

In the present work, based on the quasi-2D BGK equation, a new explicit/implicit UGKS-AS is developed for axisymmetric flow in all flow regimes. This paper is organized as following. In Section 2, the UGKS-AS for axisymmetric flow is constructed with a time evolving distribution function for the flux evaluation. In Section 3, the proposed scheme are tested in many axisymmetric flows in a wide range of Knudsen numbers. The accuracy and efficiency of the scheme is validated through many delicate challenging applications.

## 2. UGKS for axisymmetric flow

### 2.1. UGKS for 3D flow

The axisymmetric UGKS flow solver is based on the quasi-2D kinetic model in cylindrical coordinate which is a simplification of the full 3D kinetic equation. In order to understand the contracting formulation, the UGKS in a 3D Cartesian coordinate system is briefly described first.

The 3D BGK equation in Cartesian coordinates is

$$\frac{\partial f}{\partial t}+u\frac{\partial f}{\partial x}+v\frac{\partial f}{\partial y}+w\frac{\partial f}{\partial z}=\frac{g-f}{\tau}, \tag{1}$$

$$g=\rho\left(2\pi RT\right)^{-\frac{3+K}{2}}\mathrm{e}^{-\frac{1}{2RT}\left((u-U)^2+(v-V)^2+(w-W)^2+\xi^2\right)},$$

where $f$ is the particle distribution function, $g$ is the Maxwellian equilibrium state determined by the local macro flow variables, i.e., density $\rho$, temperature $T$, and velocities $U, V, W$. Here $\tau$ is the particle mean collision time, $R$ is the gas constant, and $\boldsymbol{\xi}$ is the internal variable with $K$ degrees of freedom, such as molecular rotation and vibration.

To construct the numerical scheme, the physical space $(x, y, z)$ and velocity space $(u, v, w)$ are discretized into $N_iN_jN_k$ and $N_lN_sN_q$ computational cells, respectively, indexed by $(i, j, k)$ and $(l, s, q)$. The cell averaged distribution function is

recorded as $f^n_{ijklsq}$ and the corresponding macroscopic conservative variables $\mathbf{W}^n_{ijk} = (\rho, \rho U, \rho V, \rho W, \rho E)^{\mathrm{T}}$ at time $t = t^n$, which are equal to the values at the cell center for a second order finite volume scheme in the physical space. $f^n_{ijklsq}$ is also abbreviate as $f^n_{ijk}$ in the absence of ambiguity. Thus in UGKS the conservative variables and distribution function are both updated by

$$\mathbf{W}^{n+1}_{ijk} = \mathbf{W}^n_{ijk} + \frac{1}{\Omega_{ijk}} \sum_{m \in \overline{S}(i,j,k)} \Delta S_m \int_0^{\Delta t}\!\!\int u_m \widehat{f}_m[t] \boldsymbol{\Psi} \mathrm{d}\Xi \mathrm{d}t, \tag{2}$$

$$f^{n+1}_{ijk} = f^n_{ijk} + \frac{1}{\Omega_{ijk}} \sum_{m \in \overline{S}(i,j,k)} \Delta S_m \int_0^{\Delta t} u_m \widehat{f}_m[t] \mathrm{d}t + \frac{1}{\Omega_{ijk}} \int_0^{\Delta t}\int_{\Omega_{ijk}} J[f] \mathrm{d}\Omega \mathrm{d}t, \tag{3}$$

where $\boldsymbol{\Psi} = (1, u, v, w, (u^2 + v^2 + w^2 + \xi^2)/2)^{\mathrm{T}}$ is the moment vector and $\mathrm{d}\Xi = \mathrm{d}u\mathrm{d}v\mathrm{d}w\mathrm{d}\boldsymbol{\xi}$ the element of velocity space. $\overline{S}(i,j,k)$ is the index of the cell interface and $\Omega_{ijk}$ is the physical volume. $\Delta S_m$ is the area of cell interface, $\widehat{f}_m$ is the distribution function and $u_m$ is the particle velocity in the inward normal direction. $J[f] = (g - f)/\tau$ is the collision term in BGK equation. In order to simplify the notations, the time $t^n = 0$ and the interface $m = (i + 1/2, j, k)$ are used. For a directional splitting method, the distribution function at the cell interface is constructed [16,3],

$$\begin{aligned} \widehat{f}_{i+1/2,j,k}(t) &= \frac{1}{\tau}\int_0^t g(x', t')\mathrm{e}^{-(t-t')/\tau}\mathrm{d}t' + \mathrm{e}^{-t/\tau} f^n_{i+1/2,j,k}[x_{i+1/2} - u_l t], \\ x' &= x_{i+1/2} - u_l(t - t'), \end{aligned} \tag{4}$$

from the analytical solution of the BGK equation.

The first-order Taylor expansion of $f^n_{i+1/2,j,k}$ and $g$ around the cell interface $x_{i+1/2} = 0$ and time $t^n = 0$ is adopted [20] which guarantees the asymptotic approximation of NS solution. Then the distribution function at the cell interface can be obtained,

$$\begin{aligned} \widehat{f}_{i+1/2,j,k}(t) = {} & (1 - c_0) g^n_{i+1/2,j,k} + [t c_0 - \tau(1 - c_0)] u_l (\partial g/\partial x)^n_{i+1/2,j,k} + [t - \tau(1 - c_0)] (\partial g/\partial t)^n_{i+1/2,j,k} \\ & + c_0 f^n_{i+1/2,j,k} - t c_0 u_l (\partial f/\partial x)^n_{i+1/2,j,k}, \end{aligned} \tag{5}$$

where $c_0 = \mathrm{e}^{-t/\tau}$. The distribution functions and their spatial slopes at the cell interface are all computed through the piece-wise linear reconstruction. For example, the initial distribution function and its slope are reconstructed as,

$$f^n_{i+1/2,j,k} = \mathrm{H}[u_l]\left(f^n_{ijk} + \sigma^n_{ijk}\Delta x_i/2\right) + (1 - \mathrm{H}[u_l])\left(f^n_{i+1,j,k} - \sigma^n_{i+1,j,k}\Delta x_{i+1}/2\right), \tag{6}$$

$$(\partial f/\partial x)^n_{i+1/2,j,k} = \sigma^n_{i+1/2,j,k} = \mathrm{H}[u_l]\sigma^n_{ijk} + (1 - \mathrm{H}[u_l])\,\sigma^n_{i+1,j,k}. \tag{7}$$

Here $\mathrm{H}[x]$ is the Heaviside function. The slopes $\sigma^n_{ijk}$ and $\sigma^n_{i+1,j,k}$ are reconstructed with the help of van Leer limiter. The Maxwellian distribution function $g^n_{i+1/2,j,k}$ is determined by the conservative variables at cell interface,

$$\mathbf{W}^n_{i+1/2,j,k} = \int f^n_{i+1/2,j,k} \boldsymbol{\Psi} \mathrm{d}\Xi. \tag{8}$$

The spatial and temporal slopes of the equilibrium state are written as $\partial g/\partial x = ag$, $\partial g/\partial t = Ag$, where $a = \mathrm{H}[u_l]a^L + (1 - \mathrm{H}[u_l])a^R$, $a^{L,R} = a^{L,R}_\alpha \Psi_\alpha$, $A = A_\alpha \Psi_\alpha$, $\alpha = 1 - 5$. These local coefficients $a^{L,R}_\alpha$, $A_\alpha$ are fully determined by the reconstructed spatial slopes of macroscopic variables. Details can be found in the literature [15].

Consequently, the integral of the distribution function for flux calculation is constructed as

$$\int_0^{\Delta t} \widehat{f}_{i+1/2,j,k}\mathrm{d}t = c_1 g^n_{i+1/2,j,k} + c_2 a u_l g^n_{i+1/2,j,k} + c_3 A g^n_{i+1/2,j,k} + c_4 f^n_{i+1/2,j,k} + c_5 u_l \sigma^n_{i+1/2,j,k}, \tag{9}$$

$$\begin{aligned} & c_4 = \tau(1 - \mathrm{e}^{-\Delta t/\tau}), \quad c_5 = \tau\Delta t - (\tau + \Delta t)c_4, \\ & c_1 = \Delta t - c_4, \quad c_2 = -\tau c_1 - c_5, \quad c_3 = \Delta t^2/2 - \tau c_1. \end{aligned}$$

The key for UGKS to recover the NS solutions in the continuum regime is the use of the integral solution for BGK equation in flux evaluation, which couples the particle free transport, represented by the convection terms, and collisions [20]. The integral solution covers the flow physics from the molecular free transport to the equilibrium state evolution. The regime represented by the integral solution depends on the ratio of the time step $\Delta t$ and the local particle collision time, with the limiting solutions of free transport ($\Delta t \ll \tau$) and NS flux ($\Delta t \gg \tau$).

To develop a scheme for all flow regimes based on the quasi-2D equation for axisymmetric flow is a difficult task due to the additional source terms in cylindrical coordinates and its coupling with particle transport and collision.

### 2.2. Transformation from Cartesian to cylindrical coordinates

In this section, the kinetic equation in cylindrical coordinate system will be presented. All convection terms in the axisymmetric quasi-2D model can be obtained by coordinate transformation from the full 3D kinetic model. The cylindrical coordinates $(x', r', \theta', u', \zeta', \omega')$ and the partial derivatives are

$$\begin{pmatrix} x \\ y \\ z \end{pmatrix} = \begin{pmatrix} x' \\ r'\cos\theta' \\ r'\sin\theta' \end{pmatrix}, \quad \begin{pmatrix} u \\ v \\ w \end{pmatrix} = \begin{pmatrix} u' \\ \zeta'\cos(\theta'+\omega') \\ \zeta'\sin(\theta'+\omega') \end{pmatrix},$$
$$\begin{pmatrix} \frac{\partial}{\partial x} \\ \frac{\partial}{\partial y} \\ \frac{\partial}{\partial z} \end{pmatrix} = \begin{pmatrix} \frac{\partial}{\partial x'} \\ \cos\theta'\frac{\partial}{\partial r'} - \frac{1}{r'}\sin\theta'\frac{\partial}{\partial\theta'} + \frac{1}{r'}\sin\theta'\frac{\partial}{\partial\omega'} \\ \sin\theta'\frac{\partial}{\partial r'} + \frac{1}{r'}\cos\theta'\frac{\partial}{\partial\theta'} - \frac{1}{r'}\cos\theta'\frac{\partial}{\partial\omega'} \end{pmatrix}. \tag{10}$$

Axial symmetry gives that unknown variables are independent of $\theta'$, which can be any value in $[0, 2\pi]$ and thus set as $\theta' = 0$ for simplicity. Without loss of generality, the following discussions are based on $f(x', r') = f(x', r', 0)$. The coordinates, derivatives and the convection terms in the BGK equation under the Cartesian coordinates are transformed to

$$\begin{pmatrix} x \\ y \\ z \end{pmatrix} = \begin{pmatrix} x' \\ r' \\ 0 \end{pmatrix}, \quad \begin{pmatrix} u \\ v \\ w \end{pmatrix} = \begin{pmatrix} u' \\ \zeta'\cos\omega' \\ \zeta'\sin\omega' \end{pmatrix},$$
$$\begin{pmatrix} \frac{\partial}{\partial x} \\ \frac{\partial}{\partial y} \\ \frac{\partial}{\partial z} \end{pmatrix} = \begin{pmatrix} \frac{\partial}{\partial x'} \\ \frac{\partial}{\partial r'} \\ -\frac{\partial}{r'\partial\omega'} \end{pmatrix}, \quad \begin{pmatrix} u\frac{\partial f}{\partial x} \\ v\frac{\partial f}{\partial y} \\ w\frac{\partial f}{\partial z} \end{pmatrix} = \begin{pmatrix} u'\frac{\partial f}{\partial x'} \\ \zeta'\cos\omega'\frac{\partial f}{\partial r'} \\ -\frac{\zeta'\sin\omega'\partial f}{r'\partial\omega'} \end{pmatrix}. \tag{11}$$

Under the cylindrical coordinates. With the above transformation, the axisymmetric BGK equation in non-conservative form becomes [1]

$$\frac{\partial f}{\partial t} + u'\frac{\partial f}{\partial x'} + \zeta'\cos\omega'\frac{\partial f}{\partial r'} - \frac{\zeta'\sin\omega'}{r'}\frac{\partial f}{\partial\omega'} = \frac{g-f}{\tau}, \tag{12}$$
$$g = \rho\,(2\pi RT)^{-\frac{3+K}{2}}\,\mathrm{e}^{-\frac{1}{2RT}\left((u'-U')^2+(\zeta'\cos\omega'-V_r')^2+(\zeta'\sin\omega'-V_\theta')^2+\boldsymbol{\xi}^2\right)}.$$

Based on the coordinate transformation with the assumption of axisymmetric flow, the spatial slopes in the 3D equation (1) can thus be expressed by the corresponding derivatives under the cylindrical coordinates. And so are the convection terms. What's remarkable is the transformation of the convection term in the $z$ direction or $w\partial f/\partial z$. As the $z$ derivative is transformed to the $\omega'$ derivative divided by negative $r'$, this convection term is transformed to the axisymmetric source term $-\zeta'\sin\omega'\partial f/(r'\partial\omega')$. The quasi-2D equation (12) is formally different in type with the 3D equation because the source term cannot be solved as a convection term any more. Whatever the coordinate system is used, the physical mechanism remains the same. The distribution function is unique at any location in space and time, and the particle free transport needs to be coupled with collision in the time evolution process. Consequently, the integral solution of BGK equation is still needed for the flux evaluation with the additional consideration of the source term. Therefore, the UGKS for the quasi-2D model will be constructed with the help of time evolving solution from the integral solution of the 3D BGK model in the local Cartesian coordinates to include all physical effect of convection, source, and collision.

### 2.3. UGKS for non-conservative quasi-2D equation

With the help of coordinate transformations in Eq. (11), UGKS for the axisymmetric flow is firstly developed based the non-conservative model equation (12). Besides the well-defined UGKS formulation, the numerical discretization of the additional source term will be very important for the accuracy of the scheme.

To construct a unified scheme for equation (12), the physical plane $(x', r')$ in the cylindrical coordinates needs to be discretized. The computational cell is indexed as $(i', j')$, along with the index $(l', s', q')$ in the velocity space $(u', \zeta', \omega')$ respectively. For UGKS, the cell averaged conservative variables $\mathbf{W} = (\rho, \rho U, \rho V_r, \rho V_\theta, \rho E)^{\mathrm{T}}$ and distribution function are updated by

$$\mathbf{W}_{i'j'}^{n+1} = \mathbf{W}_{i'j'}^{n} + \frac{1}{\Omega_{i'j'}} \sum_{m\in\overline{S}(i',j')} \Delta S_m \int_0^{\Delta t}\!\!\int u'_m \widehat{f}_m[t]\boldsymbol{\Psi}\mathrm{d}\Xi\mathrm{d}t + \frac{1}{r'_{i'j'}} \int_0^{\Delta t}\!\!\int \Big(-\cos\omega', -u'\cos\omega', -\zeta'\cos 2\omega', -\zeta'\sin 2\omega', -\frac{1}{2}(u'^2+\zeta'^2+\boldsymbol{\xi}^2)\cos\omega'\Big)^{\mathrm{T}} \zeta' f \mathrm{d}\Xi\mathrm{d}t, \tag{13}$$

$$f_{i'j'}^{n+1} = f_{i'j'}^{n} + \frac{1}{\Omega_{i'j'}} \sum_{m'\in\overline{S}(i',j')} \Delta S_{m'} \int_0^{\Delta t} u'_{m'} \widehat{f}_{m'}[t]\mathrm{d}t + \frac{1}{\Omega_{i'j'}} \int_0^{\Delta t}\!\!\int_{\Omega_{i'j'}} \left(\frac{\zeta'\sin\omega'}{r'}\frac{\partial f}{\partial\omega'}\right)\mathrm{d}\Omega\mathrm{d}t + \frac{1}{\Omega_{i'j'}} \int_0^{\Delta t}\!\!\int_{\Omega_{i'j'}} J[f]\mathrm{d}\Omega\mathrm{d}t. \tag{14}$$

Here the element in velocity space and moment vector are $\mathrm{d}\Xi = \zeta'\mathrm{d}u'\mathrm{d}\zeta'\mathrm{d}\omega'\mathrm{d}\boldsymbol{\xi}$ and $\boldsymbol{\Psi} = (1, u', \zeta'\cos\omega', \zeta'\sin\omega', (u'^2+\zeta'^2+\boldsymbol{\xi}^2)/2)^{\mathrm{T}}$, respectively. $u'_{m'}$ is the particle velocity in the inward normal direction and $\Delta S_{m'}$ is the length of cell interface.

The key of the UGKS is to couple the particle free transport and collision in the flux evaluation at a cell interface. Theoretically, we need to get the analytic solution of BGK equation in the cylindrical coordinates directly, including the effect from the free transport, collision, and the source term. But, it is difficult to derive the analytical solution of BGK equation directly, especially to take into account the curved particle trajectory in the cylindrical coordinates. Since the distribution function is a physical quantity and it does not change with coordinates transformation, an alternative method is to use the analytical solution in the local 3D Cartesian coordinates, and rewrite it with the cylindrical coordinates, with the consideration of particle velocity and the slopes of distribution function between these two coordinates, such as $(u_l, v_s, w_q) = (u'_{l'}, \zeta'_{s'}\cos\omega'_{q'}, \zeta'_{s'}\sin\omega'_{q'})$ and $\partial/\partial x = \partial/\partial x'$, $\partial/\partial y = \partial/\partial r'$. It is emphasized the local analytic solution in the cylindrical coordinates isn't directly derived from the axisymmetric BGK equation, but approximated from the analytical solution in the 3D Cartesian coordinate. Based on coordinate transformations, the derivations to develop the local analytic solution in the flux and axisymmetric source term evaluations are shown as follows.

For a directional splitting method, only normal slope is required in the analytical solution at a cell interface. The time evolution of $\widehat{f}_{m'}$ in Eqs. (13) and (14) can be constructed similarly as that in Eq. (9). For the axisymmetric source term coming from the convection term in the $z$ direction, a similar local analytic solution in this direction for $f$ can be obtained,

$$\int_0^{\Delta t} f_{i'j'}\mathrm{d}t = c_1 g_{i'j'}^n + c_2 w_{q'}(\partial g^n/\partial z)_{i'j'} + c_3(\partial g^n/\partial t)_{i'j'} + c_4 f_{i'j'}^n + c_5 w_{q'}(\partial f^n/\partial z)_{i'j'}. \tag{15}$$

According to the coordinate transformation Eq. (11), $w_{q'} = \zeta'_{s'}\sin\omega'_{q'}$ and the $z$ slope in the integral solution is approximated as

$$\left(\frac{\partial g^n}{\partial z}\right)_{i'j'} = -\left(\frac{1}{r'}\frac{\partial g^n}{\partial\omega'}\right)_{i'j'} = -\frac{1}{r'_{i'j'}}\left(\overline{D}g_{i'j'}^n\right)_{q'} + \frac{1}{r'}O(\Delta\omega'^{\bar{s}}),$$
$$\left(\frac{\partial f^n}{\partial z}\right)_{i'j'} = -\left(\frac{1}{r'}\frac{\partial f^n}{\partial\omega'}\right)_{i'j'} = -\frac{1}{r'_{i'j'}}\left(\overline{D}f_{i'j'}^n\right)_{q'} + \frac{1}{r'}O(\Delta\omega'^{\bar{s}}), \tag{16}$$

where $\overline{D}$ is a difference operator to approximate the partial derivative in $\omega$, with $\bar{s}$-order accuracy. Thus similar method as that in the Cartesian coordinates can be applied to determine the local coefficients in the above equation. Then the source term in Eq. (14) can be approximated as

$$\frac{1}{\Omega_{i'j'}} \int_0^{\Delta t}\!\!\int_{\Omega_{i'j'}} \left(\frac{\zeta'\sin\omega'}{r'}\frac{\partial f}{\partial\omega'}\right)\mathrm{d}\Omega\mathrm{d}t = \frac{\zeta'_{s'}\sin\omega'_{q'}}{r'_{i'j'}}\overline{D}\left(\int_0^{\Delta t} f_{i'j'}\mathrm{d}t\right)_{q'} + \frac{1}{r'}O\left(\Delta x^2, \frac{\Delta r^2}{r'^2}, \Delta\omega'^{\tilde{s}}\right). \tag{17}$$

Considering the coordinate transformation and the slopes in the $z$ direction in Eq. (16), the time integration of $f_{i'j'}$ in the source term, i.e., Eq. (15), is finally written as

$$\int_0^{\Delta t} f_{i'j'}\mathrm{d}t = c_1 g^n_{i'j'} - c_2 \frac{\zeta'_{s'}\sin\omega'_{q'}}{r'_{i'j'}}\overline{D}\left(g^n_{i'j'}\right)_{q'} + c_3 A g^n_{i'j'} + c_4 f^n_{i'j'} - c_5 \frac{\zeta'_{s'}\sin\omega'_{q'}}{r'_{i'j'}}\overline{D}\left(f^n_{i'j'}\right)_{q'}. \tag{18}$$

A typical choice of $\overline{D}$ in the source term to preserve the conservation laws of macroscopic conservative variables is the trigonometric operator developed by Mieussens [1], for example the T-CNCE:

$$\overline{D}(f)_{q'} = \frac{f_{q'+1} - f_{q'-1}}{2\sin\Delta\omega'}, \tag{19}$$

with truncation error $O(\Delta\omega'^2)$, which is used in the present work. Discrete velocity points in $\omega'$ must be uniform and the rectangular formula is used to integrate over $\omega'$ to preserve the conservation laws of the source term. Although higher-order difference operators can be constructed, it is promoted by Mieussens that trigonometric operators satisfy the conservation laws to permit robust results even with low resolution velocity mesh, which is promising to improve the efficiency of the quasi-2D models in practical applications. The collision term in Eq. (14) is approximated with semi-implicit difference scheme [15] and thus the second order accuracy in time can be achieved.

It should be mentioned that the above-mentioned UGKS is based on quasi-2D equation (12) in non-conservative form. The conservation preserving, which is important for the accuracy and robustness, is not satisfactory in many typical applications in both the present and existing studies [1]. Thus it is not further discussed in the following for conciseness. Although difficult, it is still promising to be improved if a better discretization operator on the axisymmetric source term is found. Now it is necessary to construct a numerical scheme based on the model equation in a conservative form which is of great interest in the present study. With no much difference from the above formulation, the development of UGKS based on a conservative form is straightforward.

### 2.4. UGKS-AS for axisymmetric flow

The commonly used quasi-2D model in conservative form is

$$\frac{\partial(r'f)}{\partial t} + u'\frac{\partial(r'f)}{\partial x'} + \zeta'\cos\omega'\frac{\partial(r'f)}{\partial r'} - \zeta'\frac{\partial(f\sin\omega')}{\partial\omega'} = r'\frac{g-f}{\tau}. \tag{20}$$

In the UGKS for the above equation, the cell averaged macroscopic variables are updated with the same formula (13) and the cell averaged distribution function $f_{i'j'}$ is updated as

$$\begin{aligned} f^{n+1}_{i'j'} = f^n_{i'j'} &+ \frac{1}{r'_{i'j'}\Omega_{i'j'}}\sum_{m'\in\overline{S}(i',j')}\Delta S_{m'}\int_0^{\Delta t} r'_{m'}u'_{m'}\widehat{f}_{m'}[t]\mathrm{d}t \\ &+ \frac{1}{r'_{i'j'}\Omega_{i'j'}}\int_0^{\Delta t}\int_{\Omega_{i'j'}} \zeta'\frac{\partial(f\sin\omega')}{\partial\omega'}\mathrm{d}\Omega\mathrm{d}t \\ &+ \frac{1}{r'_{i'j'}\Omega_{i'j'}}\int_0^{\Delta t}\int_{\Omega_{i'j'}} r' J[f]\mathrm{d}\Omega\mathrm{d}t. \end{aligned} \tag{21}$$

Then similar procedure in the previous section can be adopted to approximate the distribution at cell interface $\widehat{f}_{m'}$ and for the axisymmetric source term through the analytical solution of BGK equation in local Cartesian coordinates. However, in comparison with the scheme in non-conservative form, two different points should be emphasized. The first one is the construction of the analytical solution of the local 3D BGK equation. In the conservative BGK equation (20), part of the convection terms in $r'$ direction, i.e., $f\zeta'\cos\omega'$, comes from the convection in the local $z$ direction from the original non-conservative equation. Theoretically, the evaluation of this term is better to use the slope of distribution function in the $z$ direction in the analytical solution. However, in the current study, a simple directional splitting method is applied and the variation in the $z$ direction is not taken into account in the determination of the distribution function at the $r'$ interface. It is noted the local $z$ direction corresponds to the circumferential direction and the flow variations in this direction are zero according to the axial symmetry. This simplification has consequently no effect on the numerical solutions. The second one is the source term in Eq. (21) which can be approximated by

$$\frac{1}{r'_{i'j'}\Omega_{i'j'}}\int_0^{\Delta t}\int_{\Omega_{i'j'}}\zeta'\frac{\partial(f\sin\omega')}{\partial\omega'}\mathrm{d}\Omega\mathrm{d}t=\frac{\zeta'_{s'}}{r'_{i'j'}}D\left(\sin\omega'\int_0^{\Delta t}f_{i'j'}\mathrm{d}t\right)_{q'}+\frac{1}{r'}O\left(\Delta x'^2,\Delta r'^2,\Delta\omega'^{\hat{s}}\right). \tag{22}$$

The time evolution of $f_{i'j'}$ is also approximated similar to Eq. (15). The trigonometric operator is used to approximate $\partial(\sin\omega' f)/\partial\omega'$. For example, the central difference T-CCE [1]

$$D(\sin\omega' f)_{q'}=\frac{(\sin\omega' f)_{q'+1}-(\sin\omega' f)_{q'-1}}{2\sin(\Delta\omega')} \tag{23}$$

is adopted with second-order accuracy. For hypersonic flow, the compromise between robustness and accuracy may prefer the first-order upwind T-UCE [1],

$$D(\sin\omega' f)_{q'}=\frac{(\sin\omega' f)_{q'+1/2}-(\sin\omega' f)_{q'-1/2}}{2\sin(\Delta\omega'/2)}, \tag{24}$$

where

$$\begin{aligned}(\sin\omega' f)_{q'+1/2}&=(\sin\omega')^{+}_{q'+1/2}f_{q'+1}+(\sin\omega')^{-}_{q'+1/2}f_{q'},\\ (\sin\omega')^{\pm}&=\frac{1\pm\mathrm{sign}[\sin\omega']}{2}\sin\omega',\end{aligned} \tag{25}$$

and sign[$x$] is the signal function.

For curvilinear computational grids, only the flux evaluation in Eq. (21) requires modification. For simplicity and without confusions, we now omit the superscript ($'$) because all the variables are under the cylindrical coordinates in the following. The particle velocity $u_m$ normal to the cell interface is transformed to a local coordinates $(\varsigma,\eta)$ as $(u,\zeta\cos\omega)\cdot(\partial\varsigma/\partial x,\partial\varsigma/\partial r)$ in flux evaluation along $\varsigma$, and $(u,\zeta\cos\omega)\cdot(\partial\eta/\partial x,\partial\eta/\partial r)$ along $\eta$. The spatial slopes in $\widehat{f}_m$ given by Eq. (9) are also transformed to the local coordinates. The source term evaluation remains the same as Eq. (22).

Define the time averaging of arbitrary variable $h$ as $\overline{h}^n=\int_0^{\Delta t}h[t]\mathrm{d}t/\Delta t$. The macroscopic conservative variables $\mathbf{W}$ are finally updated by

$$\begin{aligned}\mathbf{W}_{ij}^{n+1}&=\mathbf{W}_{ij}^{n}+\beta\sum_{m\in\overline{S}(i,j)}J_m\mathbf{T}_m\overline{\mathbf{F}}_m^n+\alpha\overline{\mathbf{S}}_{ij}^n,\\ \mathbf{F}_m(t)&=\int u_m\widehat{f}_m[t]\mathbf{\Psi}_m\mathrm{d}\Xi,\\ \mathbf{S}&=\int(0,0,\sin\omega,-\cos\omega,0)^{\mathrm{T}}f\zeta^2\sin\omega\mathrm{d}\Xi,\end{aligned} \tag{26}$$

where $J_m=r_m\Delta S_m,\alpha=\Delta t/r_{ij},\beta=\alpha/\Omega_{ij}$. $\mathbf{T}_m$ is the transformation matrix from the local to the global coordinates. $\mathbf{\Psi}_m$ is the moment vector under the local coordinates. $\mathbf{S}$ is the macroscopic source term. The integral of $\widehat{f}_m$ in the macroscopic flux evaluation $\overline{\mathbf{F}}_m^n$ is given by Eq. (9). The time evolution of $f_{ij}$ in the macroscopic source term $\overline{\mathbf{S}}_{ij}^n$ is given by Eq. (18).

For the update of the distribution function, the semi-implicit scheme is adopted to approximate the collision term in Eq. (21) [15]:

$$\frac{1}{r_{ij}\Omega_{ij}}\int_0^{\Delta t}\int_{\Omega_{ij}}rJ[f]\mathrm{d}\Omega\mathrm{d}t=\frac{\Delta t}{2}\left(\frac{g_{ij}^n-f_{ij}^n}{\tau_{ij}^n}+\frac{g_{ij}^{n+1}-f_{ij}^{n+1}}{\tau_{ij}^{n+1}}\right)+\frac{1}{r}O\left(\Delta x^2,\Delta r^2,\Delta t^2\right), \tag{27}$$

where $g_{ij}^{n+1}$ and $\tau_{ij}^{n+1}$ are given by $\mathbf{W}_{ij}^{n+1}$. The distribution function is finally updated as

$$f_{ij}^{n+1}=\left(1+\frac{\Delta t}{2\tau_{ij}^{n+1}}\right)^{-1}\left(f_{ij}^n+\beta\sum_{m\in\overline{S}(i,j)}J_m u_m\overline{\widehat{f}}_m^n+\alpha\zeta_s D\left(\sin\omega\overline{f}_{ij}^n\right)_q+\frac{\Delta t}{2}\left(\frac{g_{ij}^n-f_{ij}^n}{\tau_{ij}^n}+\frac{g_{ij}^{n+1}}{\tau_{ij}^{n+1}}\right)\right). \tag{28}$$

Here $\overline{\widehat{f}}_m^n$ is the time integration in Eq. (9) divided by $\Delta t$, and $\overline{f}_{ij}^n$ is computed by Eq. (18) and averaged within $\Delta t$.

The local time step is introduced for the steady state computation. In each control volume $\Omega_{ij}$, the time step is given by the stability condition:

$$\Delta t=\mathrm{CFL}/\max\left(|\lambda_{ij}^{\varsigma}|_{max}+|\lambda_{ij}^{\eta}|_{max},\frac{w_{max}}{r_{ij}\Delta\omega}\right), \tag{29}$$

where

$$|\lambda_{ij}^{\varsigma}|_{max} = |\varsigma_x u_{max} + \varsigma_y v_{max}|_{ij}, |\lambda_{ij}^{\eta}|_{max} = |\eta_x u_{max} + \eta_y v_{max}|_{ij},$$
$$(\varsigma_x)_{ij} = \frac{(\Delta y)_{i-1/2,j} + (\Delta y)_{i+1/2,j}}{2\Omega_{ij}}, (\varsigma_y)_{ij} = -\frac{(\Delta x)_{i-1/2,j} + (\Delta x)_{i+1/2,j}}{2\Omega_{ij}},$$
$$(\eta_x)_{ij} = -\frac{(\Delta y)_{i,j-1/2} + (\Delta y)_{i,j+1/2}}{2\Omega_{ij}}, (\eta_y)_{ij} = \frac{(\Delta x)_{i,j-1/2} + (\Delta x)_{i,j+1/2}}{2\Omega_{ij}}, \tag{30}$$

and $u_{max}$, $v_{max}$ and $w_{max}$ are the largest absolute discrete particle velocities of $u$, $\zeta\cos\omega$ and $\zeta\sin\omega$. For the unsteady flows, the time step is given as the global minimum one for all computational cells.

The above scheme for axisymmetric flow based on the conservative quasi-2D BGK equation is named as UGKS-AS in the present study. In the scheme, Eq. (26) is the macroscopic equation to update the conservative variables. Eq. (28) is the microscopic equation to update the distribution function. Eqs. (9) and (18) give the time evolution of the distribution function in macroscopic and microscopic flux and source term evaluations.

### 2.5. Implicit UGKS-AS

To improve the efficiency of UGKS-AS for steady state solution, the implicit scheme is developed in this study. To get high efficiency in a wide range of flow regime, the implicit technique should be implemented both on the updates of macroscopic variables and the distribution function [22]. As a result, the implicit scheme will be implemented on both Eqs. (26) and (28).

Define $\delta h^n = h^{n+1} - h^n$, the implicit macroscopic and microscopic equations for axisymmetric flow are

$$\delta \mathbf{W}_{ij}^n = \beta \sum_{m\in\overline{S}(i,j)} J_m \mathbf{T}_m \overline{\mathbf{F}}_m^{n+1} + \alpha \overline{\mathbf{S}}_{ij}^n, \tag{31}$$

$$\delta f_{ij}^n = \beta \sum_{m\in\overline{S}(i,j)} J_m u_m \overline{\overline{f}}_m^{n+1} + \alpha\zeta_s D\left(\sin\omega \overline{f}_{ij}^{n+1}\right)_q + \frac{\Delta t^i}{\tau_{ij}^{n+1}}\left(g_{ij}^{n+1} - f_{ij}^{n+1}\right), \tag{32}$$

where $\alpha = \Delta t^i / r_{ij}$, $\beta = \alpha/\Omega_{ij}$. $\Delta t^i$ is the time step of the implicit scheme. $\Delta t^i = n_t \Delta t^e$ is given where $n_t$ is usually tens or hundreds. The flux, source term, and collision term in the microscopic equation Eq. (32) are treated implicitly. The flux in the macroscopic equation Eq. (31) is implicit, while the macroscopic source term remains explicit as it hardly influences the stability according to our numerical tests. All the $n+1$ terms are to be linearized to avoid solving the nonlinear systems.

For the implicit scheme with second-order accuracy in physical space, only the first-order terms in flux evaluation are to be linearized. The second-order terms in flux evaluation are kept explicit. For the macroscopic equation, the flux $\overline{\mathbf{F}}_m^{n+1}$ is linearized as

$$\overline{\mathbf{F}}_m^{n+1} = \overline{\mathbf{F}}_m^n + \left(\mathbf{A}_{m-1/2}^{+,n}\delta\mathbf{W}_{m-1/2}^n + \mathbf{A}_{m+1/2}^{-,n}\delta\mathbf{W}_{m+1/2}^n\right),$$
$$\mathbf{A}^{\pm} = \frac{\mathbf{A} \pm |\lambda_{\mathbf{A}}|\mathbf{I}}{2}, \tag{33}$$

where $\mathbf{A}$ is given as the Euler flux Jacobin and $\lambda_{\mathbf{A}}$ is its spectral radii with the consideration of viscous effect [23]. As Zhu et al. discussed [22], in order to avoid the time-consuming linearization of $g^{n+1}$ in the collision term of the microscopic equation, the updated $\mathbf{W}_{ij}^{n+1}$ provides $g^{n+1}$ since $\mathbf{A}^{\pm}$ is an efficient approximation of $\partial\overline{\mathbf{F}}/\partial\mathbf{W}$ for the evaluation of macroscopic solutions. This approximation is valid in the near continuum flow regime as the error between $f$ and its first-order Chapman–Enskog expansion in flux evaluation, such as with the order $O(\tau^2)$, is negligible in such a regime. In the whole flow regime, the error of this approximation in flux evaluation is about $\left|\delta\overline{\mathbf{F}} - \mathbf{A}^{\pm}\delta\mathbf{W}\right| \sim O(\tau^2)\,|\delta\mathbf{W}|$. As $|\delta\mathbf{W}|$ becomes very small in convergence, this approximation is efficient and numerically valid in the whole flow regime. Define $E_{\varsigma}^{\pm1}h_i = \beta h_{i\pm1}$, $E_{\eta}^{\pm1}h_j = \beta h_{j\pm1}$, the macroscopic equation Eq. (31) becomes

$$(\mathbf{D} + \mathbf{L} + \mathbf{U})\,\delta\mathbf{W}^n = \mathbf{R}^n, \tag{34}$$
$$\mathbf{D}_{ij} = \mathbf{I} + \frac{\beta}{2}\sum_{m=\varsigma,\eta} |J_m|\,\lambda_{\mathbf{A}_{ij}}\mathbf{I},$$
$$\mathbf{L}_{ij} = -E_{\varsigma}^{-1}\left(J\mathbf{T}\widetilde{\mathbf{A}}^{+}\mathbf{T}^{-1}\right)_{i+1/2,j} - E_{\eta}^{-1}\left(J\mathbf{T}\widetilde{\mathbf{A}}^{+}\mathbf{T}^{-1}\right)_{i,j+1/2},$$
$$\mathbf{U}_{ij} = -E_{\varsigma}^{+1}\left(J\mathbf{T}\widetilde{\mathbf{A}}^{-}\mathbf{T}^{-1}\right)_{i-1/2,j} - E_{\eta}^{+1}\left(J\mathbf{T}\widetilde{\mathbf{A}}^{-}\mathbf{T}^{-1}\right)_{i,j-1/2},$$
$$\mathbf{R}_{ij}^n = \beta\sum_{m=\varsigma,\eta} J_m\mathbf{T}_m\overline{\mathbf{F}}_m^n + \alpha\overline{\mathbf{S}}_{ij}^n,$$

where $E_{\varsigma,\eta}^{\pm1}\widetilde{\mathbf{A}}^{\mp} = E_{\varsigma,\eta}^{\pm\frac{3}{2}}\mathbf{A}^{\mp}$ and $\mathbf{T}$ is the transformation matrix from local to global coordinates. $\mathbf{D}$, $\mathbf{L}$, $\mathbf{U}$ are diagonal, lower triangular, and upper triangular matrix, respectively. LU factorization [22,23] is used to obtain the increment,

$$(\mathbf{D}+\mathbf{L})\,\delta\mathbf{W}^{*}=\mathbf{R}^{n},$$
$$(\mathbf{D}+\mathbf{U})\,\delta\mathbf{W}^{n}=\mathbf{D}\delta\mathbf{W}^{*}. \tag{35}$$

$\delta\mathbf{W}_{ij}^{n}$ is solved first by a forward sweep and then a backward sweep. Then $\mathbf{W}_{ij}^{n+1}$ and $g_{ij}^{n+1}$ can be calculated through $\mathbf{W}_{ij}^{n+1}=\mathbf{W}_{ij}^{n}+\delta\mathbf{W}_{ij}^{n}$. The implicit scheme of the macroscopic equation is the traditional LU-SGS for the conservative variables. At each time step, $\mathbf{W}_{ij}^{n+1}$ has to be corrected after $f_{ij}^{n+1}$ is updated from the microscopic equation. Here $\mathbf{W}_{ij}^{n+1}$ and $g_{ij}^{n+1}$ given by the implicit scheme of the macroscopic equation are denoted as $\mathbf{W}_{ij}^{c}$ and $g_{ij}^{c}$ respectively.

For microscopic equation Eq. (32), the first-order term in $\overline{\widetilde{f}}_{m}^{n+1}$ in flux evaluation is linearized as

$$\overline{\widetilde{f}}_{m}^{n+1}=\overline{\widetilde{f}}_{m}^{n}+\left(u_{m}^{+}\delta f_{m-1/2}^{n}+u_{m}^{-}\delta f_{m+1/2}^{n}\right),$$
$$u_{m}^{\pm}=\frac{1\pm\mathrm{sign}[u_{m}]}{2}u_{m}. \tag{36}$$

In the collision term, $g_{ij}^{n+1}$ is given as $g_{ij}^{c}$, $\tau_{ij}^{c}$ from $\mathbf{W}_{ij}^{c}$. The collision term at $t^{n+1}$ is then approximated as

$$\frac{\Delta t^{i}}{\tau_{ij}^{n+1}}\left(g_{ij}^{n+1}-f_{ij}^{n+1}\right)=\frac{\Delta t^{i}}{\tau_{ij}^{c}}\left(g_{ij}^{c}-f_{ij}^{n}\right)-\frac{\Delta t^{i}}{\tau_{ij}^{c}}\delta f_{ij}^{n}. \tag{37}$$

In the source term of Eq. (32), T-UCE [1] is implemented. Similarly, only the lower-order terms in source term evaluation are to be linearized. The time evolving distribution function per unit time $\overline{f}_{q}^{n+1}$ is linearized as

$$\overline{f}_{q}^{n+1}=\overline{f}_{q}^{n}+\delta f_{q}^{n}. \tag{38}$$

Define $E_{\omega}^{\pm1}h_{q}=\chi h_{q\pm1}$, $\chi=\alpha\zeta_{s}/\left(2\sin\frac{\Delta\omega}{2}\right)$, Eq. (32) becomes

$$\left(\mathbf{D}'+\mathbf{L}'+\mathbf{U}'\right)\delta\boldsymbol{f}^{n}=\mathbf{R}'^{n}, \tag{39}$$
$$D'_{ijq}=1+\frac{\Delta t^{i}}{\tau_{ij}^{c}}+\frac{\beta}{2}\sum_{m=\varsigma,\eta}|J_{m}|\,\mathrm{sign}[u_{m}]u_{m}+\frac{\chi}{2}\sum_{m=\omega}\mathrm{sign}[\sin\omega_{m}]\sin\omega_{m},$$
$$L'_{ijq}=-E_{\varsigma}^{-1}\left(Ju^{+}\right)_{i+1/2,j,q}-E_{\eta}^{-1}\left(Ju^{+}\right)_{i,j+1/2,q}+E_{\omega}^{-1}\left(\sin\omega\right)_{i,j,q+1/2}^{-},$$
$$U'_{ijq}=-E_{\varsigma}^{+1}\left(Ju^{-}\right)_{i-1/2,j,q}-E_{\eta}^{+1}\left(Ju^{-}\right)_{i,j-1/2,q}-E_{\omega}^{+1}\left(\sin\omega\right)_{i,j,q-1/2}^{+},$$
$$R'^{n}_{ijq}=\beta\sum_{m=x,r}J_{m}u_{m}\overline{\widetilde{f}}_{m}^{n}+\alpha\zeta_{s}D\left(\sin\omega\overline{f}_{ij}^{n}\right)_{q}+\frac{\Delta t^{i}}{\tau_{ij}^{c}}\left(g_{ij}^{c}-f_{ij}^{n}\right).$$

LU factorization is also used to solve Eq. (39),

$$\left(\mathbf{D}'+\mathbf{L}'\right)\delta\boldsymbol{f}^{*}=\mathbf{R}'^{n},$$
$$\left(\mathbf{D}'+\mathbf{U}'\right)\delta\boldsymbol{f}^{n}=\mathbf{D}'\delta\boldsymbol{f}^{*}. \tag{40}$$

When $\delta f_{ij}^{n}$ is obtained, $f_{ij}^{n+1}$ can be calculated with $f_{ij}^{n+1}=f_{ij}^{n}+\delta f_{ij}^{n}$. Then $\mathbf{W}_{ij}^{c}$ can be corrected through the conservative moments of $f_{ij}^{n+1}$. To reduce the error of numerical integration, which is related to the interval or the number of discrete velocity points, the conservation constraint $\mathbf{H}=\mathbf{0}$ introduced in [24,25] is used here

$$\mathbf{H}=\sum\left(g(\mathbf{W}^{n+1})-f^{n+1}\right)\boldsymbol{\Psi}\overline{w}\zeta\,\Delta u\Delta\zeta\,\Delta\omega\Delta\boldsymbol{\xi}, \tag{41}$$

where $\overline{w}$ is the integral weight. The Newton iteration to solve $\mathbf{W}^{n+1}$ from the constraint $\mathbf{H}=\mathbf{0}$ is

$$\overline{\mathbf{M}}^{s_t}\left(\mathbf{Q}^{s_t+1}-\mathbf{Q}^{s_t}\right)=-\mathbf{H}^{s_t}, \tag{42}$$

where $\mathbf{Q}=(\rho,U,V_{r},V_{\theta},2RT)^{\mathrm{T}}$ and $\overline{\mathbf{M}}=\partial\mathbf{H}/\partial\mathbf{Q}$ is approximated with $V=V_{r},W=V_{\theta}$ for the simplicity, as Titarev did [25]. After 5 to 8 steps, the residuals usually decrease by several orders of magnitude, which is enough for the present numerical tests. $\mathbf{W}_{ij}^{n+1}$ is then corrected from the converged $\mathbf{Q}_{ij}$.

It has to be pointed out that according to the literature [22], to preserve a valid physical resolution when defining $\overline{\mathbf{F}}_{m}^{n}$, $\overline{\widetilde{f}}_{m}^{n}$ and $\overline{f}_{ij}^{n}$ in flux and source term evaluation, $\Delta t$ is actually the explicit one $\Delta t^{e}$, which is constrained by the CFL condition Eq. (29) with CFL $<1$. The $\Delta t$ used in $\alpha,\beta,\chi$ is the implicit one $\Delta t^{i}=n_{t}\Delta t^{e}$. The equivalent CFL number for the implicit scheme is then $n_{t}$ CFL.

Now $\mathbf{W}_{ij}^{n+1}$ and $f_{ij}^{n+1}$ are obtained by the implicit UGKS-AS through the macroscopic equation Eq. (35) and microscopic equation Eq. (40), together with the constraint Eq. (42) to correct $\mathbf{W}_{ij}^{n+1}$.

### 2.6. Boundary conditions

In explicit UGKS-AS, $\mathbf{W}_{ij}^n$ and $f_{ij}^n$ in the ghost cells of the physical space are given in the same way as the plane 2D flows [3]. For the discrete $\omega_q$ in $[0, 2\pi]$ at $\Delta\omega/2, \Delta\omega, ..., 2\pi - \Delta\omega/2$, because of the periodicity of trigonometric functions, $f_0^n$ and $f_{N_q+1}^n$ are

$$\begin{aligned} &f_0^n = f_{N_q}^n, \quad \omega_0 = -\Delta\omega/2, \\ &f_{N_q+1}^n = f_1^n, \quad \omega_{N_q+1} = 2\pi + \Delta\omega/2. \end{aligned} \tag{43}$$

For flow with $V_\theta = 0$, $f(\omega) = f(-\omega)$ and $\omega_q$ has discrete values on $[0, \pi]$ at $\Delta\omega/2, \Delta\omega, ..., \pi - \Delta\omega/2$:

$$\begin{aligned} &f_0^n = f_1^n, \quad \omega_0 = -\Delta\omega/2, \\ &f_{N_q+1}^n = f_{N_q}^n, \quad \omega_{N_q+1} = \pi + \Delta\omega/2. \end{aligned} \tag{44}$$

In implicit UGKS-AS, $\delta\mathbf{W}_{ij}^n$ and $\delta f_{ijq}^n$ in ghost cells need to be set. There is no special treatment for $\delta\mathbf{W}_{ij}$ and $\delta f_{ij}$, or $\delta\mathbf{W}_{ij} = 0$ and $\delta f_{ij} = 0$ are defined in ghost cells, except for outer flows when $\delta\mathbf{W}_{ij}^n$ and $\delta f_{ij}^n$ are extrapolated from $\delta\mathbf{W}_{ij}^*$ and $\delta f_{ij}^*$ in the inner cells. For the source term at $w_0$ and $w_{N_q+1}$, from Eqs. (39) and (25) they are given by

$$(\sin\omega)_{i,j,1/2}^- = 0, \quad (\sin\omega)_{i,j,N_q+1/2}^+ = 0. \tag{45}$$

As a result, at $q = 0$ and $q = N_q + 1$ we have

$$\delta f_0^n = 0, \quad \delta f_{N_q+1}^n = 0. \tag{46}$$

The values of $\delta f_0^n$ and $\delta f_{N_q+1}^n$ don't bring any numerical difference when solving the microscopic equation.

### 2.7. Remarks

In the present UGKS-AS, the time evolution of the distribution function in the source term is constructed through a directional splitting method from the analytical solution of BGK equation, and this solution can be easily deduced from the full 3D model. Since the source term has the same physical mechanism as the $z$-direction convection term in a local Cartesian coordinate system, the coupling of particle free transport and collision is included in the evaluation of the source term. The use of the integral solution (18) guarantees the recovering of the NS solutions by UGKS-AS in continuum flow regime, and it is expected that the UGKS-AS will present accurate solutions in a wide range of flow regime with high efficiency. Although the UGKS-AS is developed for BGK equation in the above sections, it can be easily extended for other BGK type models.

In the earlier UGKS approach for axisymmetric flow [26], the source term $\zeta_s D(\sin\omega \overline{f}_{ij}^n)_q \Delta t / r_{ij}$ is approximated with the first-order accuracy in time as $\zeta_s D(\sin\omega f_{ij}^n)_q \Delta t / r_{ij}$. In comparison with the current UGKS-AS, it only recovers the limiting solutions of the free transport ($\Delta t \ll \tau$) for the source term. And then $\overline{f}_{ij}^n$ is constructed as $f_{ij}^n$. No coupling effect between the particle transport and collision is included in the time evolution of the source term. Therefore, this scheme cannot present accurate NS solutions in the continuum flow regime when the time step is much larger than the particle collision time. This defect will be observed numerically in the next section.

A quasi-2D model may require more refined velocity mesh in the discretization of the $\omega$ derivative of the distribution function [1,2]. Additional computational cost will be associated with the increment of the discrete velocity points, which may weaken the efficiency of the UGKS-AS. Fortunately, owing to the satisfaction of conservation laws by the trigonometric operators [1], the UGKS-AS gives reliable results on a coarse mesh in the velocity space.

The convergence of the implicit UGKS-AS can be further improved when simulating the steady flows. However, because of the LU factorization and the requirement of boundary conditions for $\delta\mathbf{W}$ or $\delta f$, the error related to $\Delta t^i$ and extra errors from the boundary conditions are brought into the implicit scheme. The errors can damage the conservation properties and may not be acceptable, especially for cases with large $\Delta t^i$. This usually happens in flows with small variations, in which the satisfaction of conservation becomes important. The improvement of efficiency in the implicit UGKS-AS must be considered together with its accuracy when it is compared with the explicit UGKS-AS. Zhu et al. [22] discussed the non-conservation property in the implicit UGKS in the closed or open systems. A similar remark is also proposed by Mieussens about the implicit DVM with different linearization on $g^{n+1}$ [1]. On the other hand, for large variation flows the implicit UGKS-AS is expected to be acceptable with high efficiency and negligible accuracy lost from the conservation problem.

## 3. Numerical results

Several typical axisymmetric flows, such as rotating Couette flow, thermo acoustic waves between coaxial cylinders, supersonic flow past a sphere, and the force driven cylindrical Poiseuille flow, are studied by the newly developed UGKS-AS in this section to validate the scheme.

In the present simulations, the discretized velocity range is set to $[U - \alpha_{umin}U_{ref}, U + \alpha_{umax}U_{ref}]$ for $u$, and $[0, \max(|V_r|, |V_\theta|) + \alpha_{\zeta max}U_{ref}]$ for $\zeta$. $U_{ref}$ is relevant to the most probable molecular velocity. The coefficients $\alpha_{umin}, \alpha_{umax}$, and $\alpha_{\zeta max}$ for the effective range, estimated from the numerical quadrature rules [3], are all equal to or larger than 4. The velocity space is uniformly discretized. Simpson formula is used to integrate over $u$ and $\zeta$ if without specification. Unless otherwise stated, the flow variables are non-dimensional or in SI units. T-CCE is used in circumferential discretization in most cases in the present simulations for its high accuracy, except the supersonic flow past a sphere where T-UCE is used for its robustness. Parallelization in physical space is implemented in some simulations. For steady flow, the steady state is obtained after the density residual is less than $10^{-10}$.

### 3.1. Rotating Couette flow

The rotating flow between two coaxial cylinders is a well-studied benchmark test which has analytical solutions both in continuum and free molecular regime, and a large number of numerical simulations can be found in literature [9,5]. The focus here is on the accuracy of UGKS-AS in the whole flow regime with Knudsen number Kn ranged from $10^{-4}$ to $10^2$, where $\mathrm{Kn} = \lambda/r_{in}$ is defined as the ratio of mean free path and the inner cylinder radius $r_{in} = 1$, based on the average density $\rho_{av} = 1$ and wall temperature $T_w = 1$ for both cylinders.

The inner cylinder rotates at a velocity $0.1 \le V_{in}/\sqrt{2RT_w} \le 0.5$. The outer cylinder has a radius $r_o = 2$ and remains stationary. The diffusive condition is adopted at the cylinder walls. To compare the results in [5], the monatomic gas with Prandtl number $\mathrm{Pr} = 1$ and gas constant $R = 1/2$ is simulated. The viscosity coefficient is given by $\mu = \mathrm{Kn}\sqrt{\pi}RT/2$. To compare with the NS solution for incompressible continuum flow, $V_\theta/V_{in} = (4/r - r)/3$, the inner cylinder rotates at $V_{in} = 0.1$ for $\mathrm{Kn} < 0.001$.

The domain in $r$ direction is divided with 20 uniform cells. To get a grid convergent solution, the constant $\alpha_{\zeta max} = 6$ is chosen. $(31, 60)$ grids are adopted in $(\zeta, \omega)$ for $10^{-4} \le \mathrm{Kn} \le 1$, and $(41, 80)$ for $1 < \mathrm{Kn} \le 10^2$. Here $(x, u)$ are abbreviated and are not discretized. The explicit UGKS-AS is applied as it is much suitable for the capturing of small variation of flow variables. The CFL number is set to 0.4.

For $0.02 \le \mathrm{Kn} \le 10$ and $V_{in} = 0.5$, comparisons of density, temperature and velocity are shown in Fig. 1 between UGKS-AS and DVM [5]. The two sets of results are in good agreement even for the slightly variation of density and temperature. However, the schemes based on quasi-2D models are always questioned about their accuracy and efficiency compared with the full 3D models [27]. While in fact, to get a circumferential mass flux with a relative error within 5% to the grid converged result for $\mathrm{Kn} = 0.1$, only 3240 grid points in total, i.e. $(20, 9, 18)$ in $(r, \zeta, \omega)$, are required for UGKS-AS. On the contrary, it is rather difficult to realize a simulation on such coarse grids by a full 3D model in this case with at least four dimension discretization, i.e. $(y, z, v, w)$.

As shown in Fig. 2, UGKS-AS is also validated for $\mathrm{Kn} = 10^2$ to approach the free molecular limit [9] and $\mathrm{Kn} = 10^{-4}$ to approach the continuum flow limit. The temperatures in radial, circumferential, and streamwise directions, defined as $\int f((\zeta\cos\omega)^2, (\zeta\sin\omega)^2, u^2)\mathrm{d}\Xi/(\rho R)$ correspondingly, are shown in Fig. 3 for $0.1 \le \mathrm{Kn} \le 100$ with $V_{in}/U_{ref} = 0.5$. As the rarefaction effect becomes stronger, the temperatures in different directions depart from each other remarkably. The streamwise temperature even remains undisturbed in the free molecular limit.

Comparisons are also made with the original UGKS-AS [26] by constructing $\overline{f}_{ij}^n = f_{ij}^n$ in the source term. As shown in Fig. 2, although the velocity profiles agree well between the current UGKS-AS and original scheme in free molecular limit, their discrepancy in the NS limit is clear. At $\mathrm{Kn} = 10^{-4}$, we have $\Delta t \approx 30\tau$. When $\Delta t$ is much larger than $\tau$, the error in the original scheme [26] from its inappropriate time evolution for the source term emerges. The result verifies that the use of the integral solution which couples the particle free transport and collision when discretizing the source term is necessary for its asymptotic recovering of NS solutions. Unfortunately, most AP schemes in literatures are still based on the decoupled approach for the particle transport and collision. For the extension of UGKS to more complex systems, it is also emphasized that for a physically validated extension all source term discretization should consider the time evolving solution of the full model equation with coupled transport and collision.

### 3.2. Thermo acoustic waves between coaxial cylinders

As the time step of UGKS-AS is not constrained by the particle collision time, the unsteady simulations by UGKS-AS can be easily carried out for the thermo acoustic waves between coaxial cylinders [28–30]. The thermo acoustic waves induced by a sudden change of circumferential velocity are simulated with the explicit UGKS-AS from the initial to the final steady state. The time varying results of UGKS-AS will be compared with the existing NSF and DSMC results [28].

The hard sphere monatomic gas is simulated with the Shakhov model for $\mathrm{Pr} = 2/3$ and $R = 1/2$ [31]. The radius is $r_{in} = 1$ for inner cylinder and $r_o = 2$ for the outer one. The velocities of the cylinders are set as $(V_{in}, V_{out})/\sqrt{2RT_w} = (0, 1)$ for $t \le 50$ and $(0, -1)$ for $t > 50$ (Case 4 in [28]). The cylinder walls are diffusive and isothermal with constant temperature $T_w = 1$. The Knudsen number $\mathrm{Kn} = \lambda/r_{in} = 0.02$ is considered here, in which the mean free path is calculated with $T_w$ and average density between the cylinders.

The computational domain in $r$ direction is divided into 240 uniform cells to capture the wall effect accurately. The number of grid points is about 0.45 million in total, $(240, 31, 60)$ in $(r, \zeta, \omega)$ with $\alpha_{\zeta max} = 6$. The unsteady simulation from $t = 0$ to $t = 100$ takes about total 24 hours of CPU time on Tianhe-2 supercomputer using 24 cores. The results of UGKS-AS

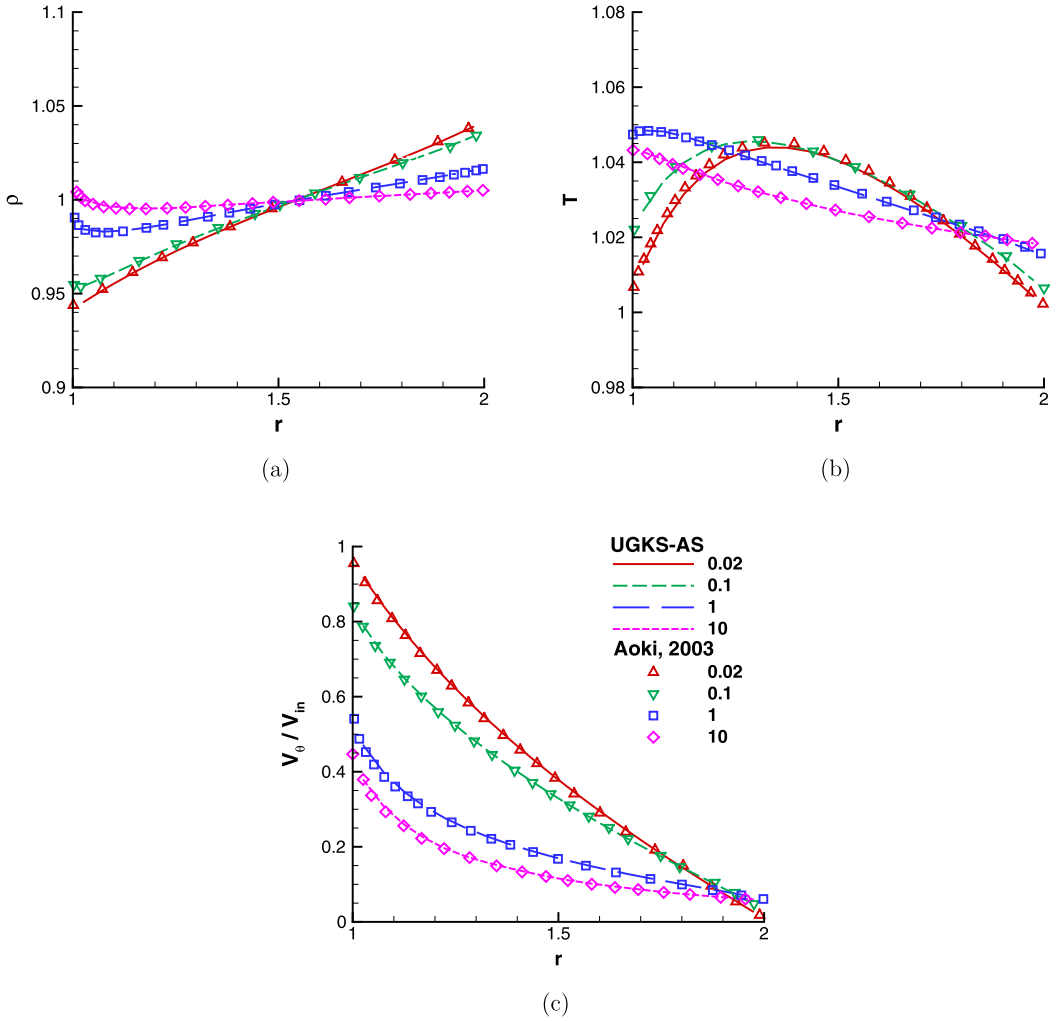


**Fig. 1.** (a) Density; (b) temperature; (c) circumferential velocity profiles for rotating Couette flow at Kn = 0.02, 0.1, 1, 10. Lines: UGKS-AS; symbols: DVM [5].

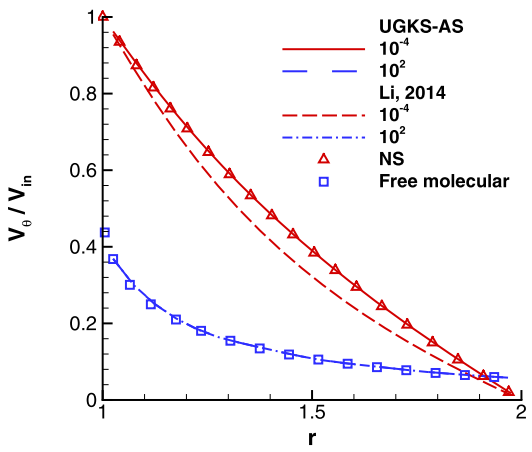


**Fig. 2.** Circumferential velocity profiles for rotating Couette flow at $Kn = 10^{-4}$ and $Kn = 10^{2}$.

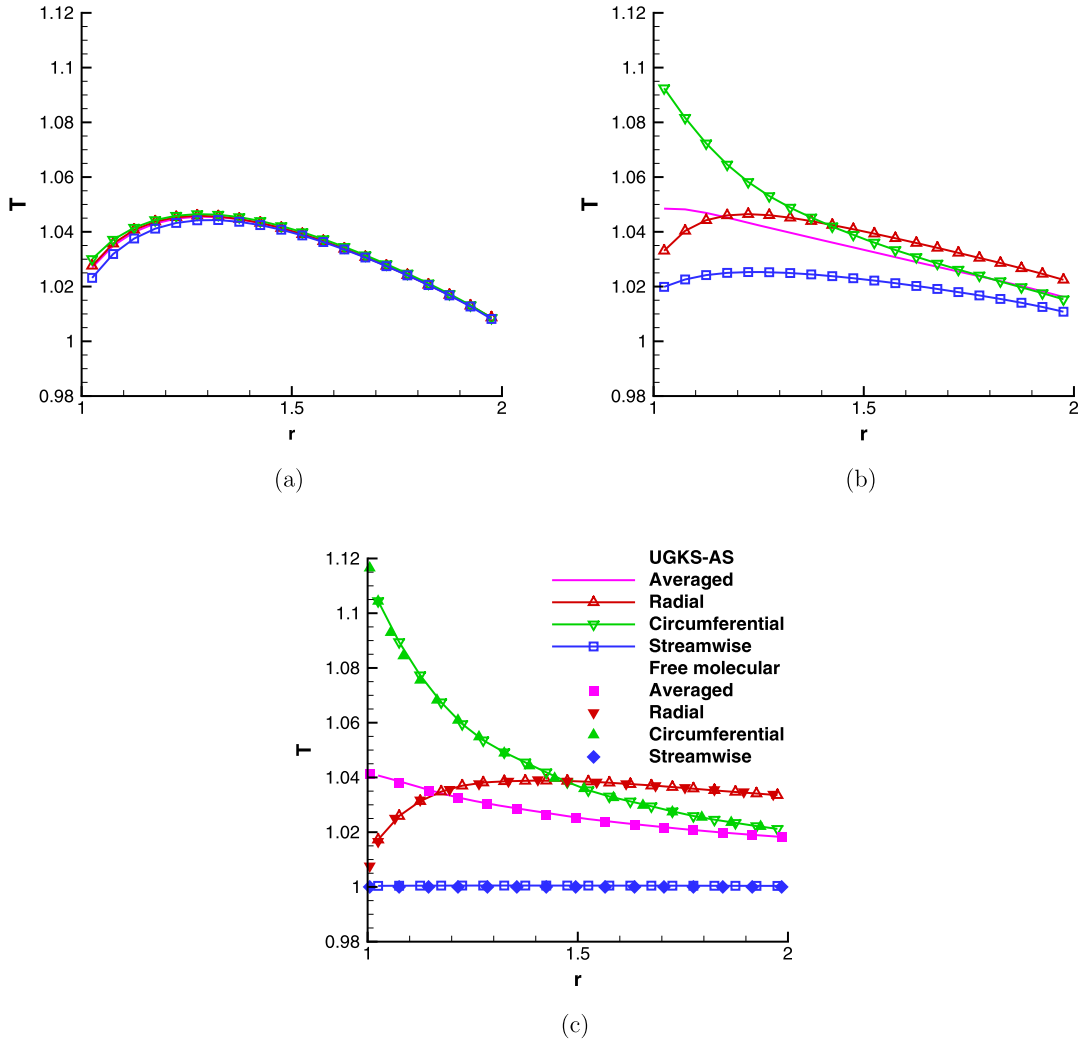


**Fig. 3.** Averaged temperature and the temperatures in the radial, circumferential and streamwise directions in rotating Couette flow at (a) Kn = 0.1; (b) Kn = 1; (c) Kn = 100.

for the time-varying wall heat flux with coarser grids (120, 31, 60) and refined (240, 61, 100) are compared in Fig. 4, which validate the grid independent result of UGKS-AS.

The predicted $V_\theta$, pressure, and temperature at different times are shown in Fig. 5. An overall good agreement between UGKS-AS and DSMC [28] is observed, while there exists some discrepancy in temperature and pressure profiles, as in Figs. 5(b), (c) at $t = 51.25$, especially near the outer cylinder. When compared with the results simulated by hydrodynamic method with first-order slip boundary condition (NSF) [28], larger discrepancy up to relative 10% can be observed near the outer cylinder for $r > 1.8$. The local Knudsen number $\mathrm{Kn}_L$ defined by the temperature slope can be considered to illustrate this discrepancy. As shown in Fig. 6, $\mathrm{Kn}_L$ increases to about 0.1 near the outer cylinder at $t = 51.25$ just after the sudden velocity change, then it is difficult for NSF to capture the rarefaction effect. In fact, $\mathrm{Kn}_L$ is also not small near the inner cylinder. This leads to evident discrepancy in heat flux at $t = 51.25$, as shown in Fig. 7, although the shear stress agrees well. It should be noted that some difference between the present predicted heat flux and DSMC simulations can be observed especially for the peak values at $t = 51.25$. The difference between BGK-type model and full Boltzmann equation may contribute to this discrepancy. Considering that the present UGKS-AS results are grid converged, further study is required.

### 3.3. Flow past a sphere

The implicit UGKS-AS is used to simulate the supersonic flow past a sphere or a half-sphere, which is a typical high-speed rarefied flow in engineering applications. The accuracy and efficiency is of main interest in this case.

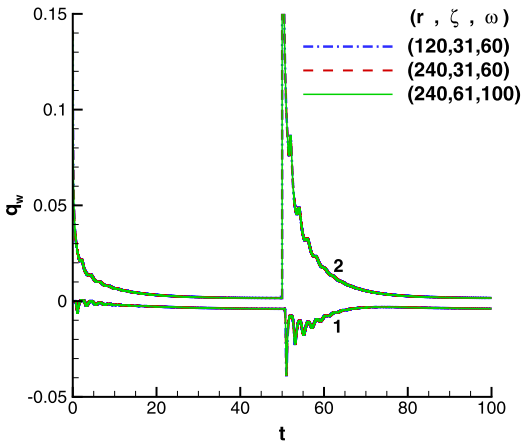


**Fig. 4.** Heat flux under different grids for a sudden circumferential velocity change at 1: inner cylinder; 2: outer cylinder.

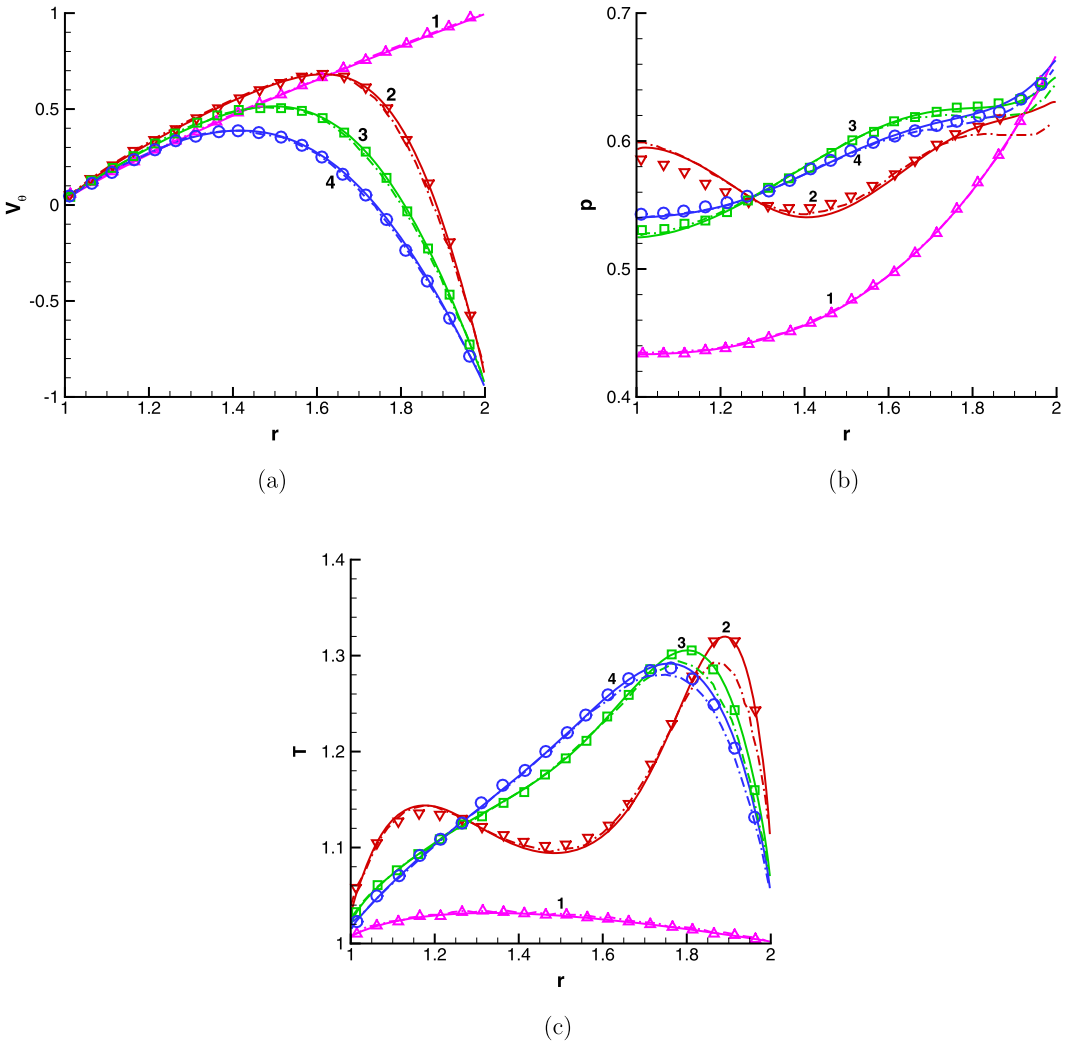


**Fig. 5.** Instantaneous (a) $V_\theta$, (b) pressure, and (c) temperature profiles at times 1: $t = 49.75$; 2: $t = 51.25$; 3: $t = 52.75$; 4: $t = 54.25$. Solid lines: UGKS-AS; dashed lines: NSF; symbols: DSMC [28].

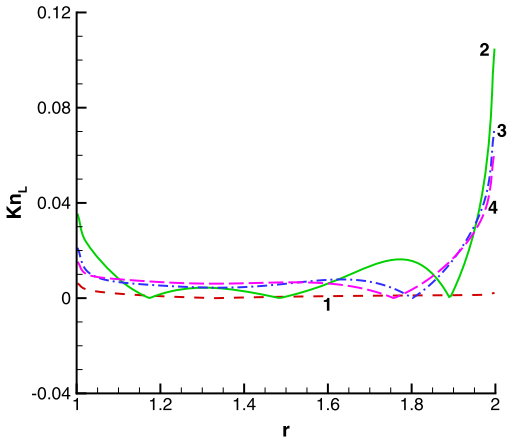


**Fig. 6.** $\mathrm{Kn}_L$ for a sudden circumferential velocity change at times 1: $t = 49.75$; 2: $t = 51.25$; 3: $t = 52.75$; 4: $t = 54.25$.

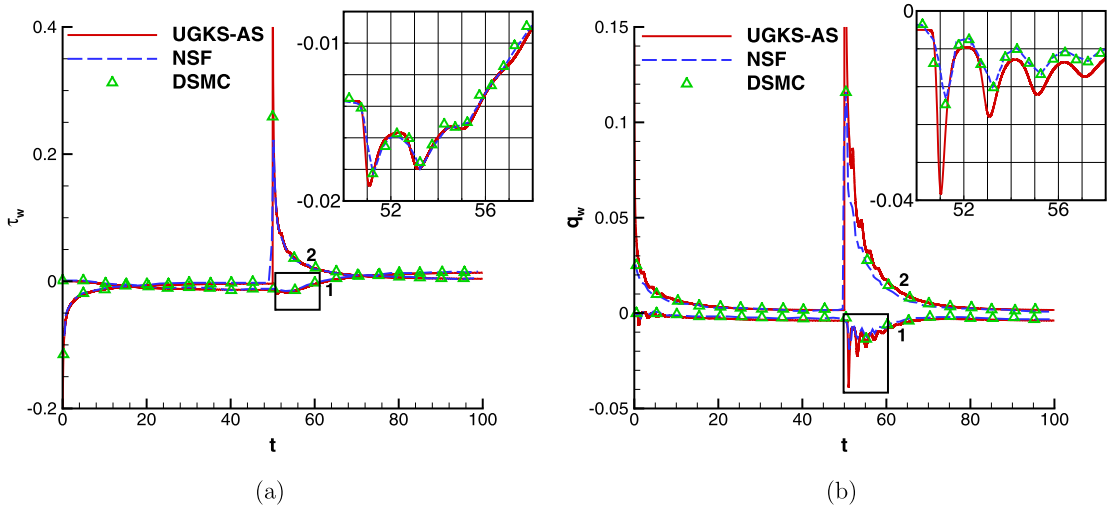


**Fig. 7.** (a) Wall shear stress and (b) heat flux at 1: inner cylinder; 2: outer cylinder.

To compare the DVM results of Mieussens [1], VHS monatomic gas with viscosity exponent 0.81 and Prandtl number $\mathrm{Pr} = 1$ is simulated. The upstream flow density $\rho_\infty = 3.17 \times 10^{-6}$, temperature $T_\infty = 249$ and velocity $U_\infty = 1504.3$ corresponding to $\mathrm{Ma} = 5$ and $\mathrm{Kn} = 0.118$ based on the sphere diameter $2r_s = 0.2$. The solid wall is diffusive and isothermal with temperature $T_w = T_\infty$.

The physical space is discretized into 60 uniform cells in the circumferential direction and 50 in the radial direction with the smallest size 0.002 and stretching ratio 1.04. The velocity mesh points are $(11, 9, 21)$ for $u \in [-2300, +2300]$, $\zeta \in [0, +2000]$, $\omega \in [0, \pi]$, respectively, the same as Mieussens' simulation. The rectangle formula is used to integrate over the velocities. The time step is set as $\Delta t^i = n_t \Delta t^e$ with $n_t = 200$ and $\mathrm{CFL} = 0.8$ for $\Delta t^e$. Five Newton iteration steps in the correction procedure are used when the iteration residuals in most flow regime decrease by five orders of magnitude. The results are found with negligible difference when compared with those using larger time steps. The results are converged when the residual given by the $L_2$-norm of relative density change in each time step, as a representative, decreases by eight orders of magnitude. All the simulations in this case are done on a single processor with Intel(R) Core(TM) i7-4790K @4.0 GHz.

The temperature contours predicted by implicit UGKS-AS are compared with those from explicit UGKS-AS in Fig. 8. A good agreement can be observed. In this high-speed external flow, the free stream is dominant and the flow field are of large variations. Consequently, the conservation properties are expected to be less crucial, thus the implicit UGKS-AS is expected to be more efficient. The efficiency of implicit UGKS-AS under different $n_t$ is shown in Fig. 9 and Table 1, with the comparison of the explicit scheme. Because the CPU time of implicit UGKS-AS for each step is 23% larger than explicit UGKS-AS, the implicit UGKS-AS under $n_t = 1$ (186 min, 5601 steps) has 10% more CPU time cost, but 11% less steps than explicit UGKS-AS. As shown in Table 1, when $n_t$ increases, the acceleration rate increases gradually, up to about 25 times

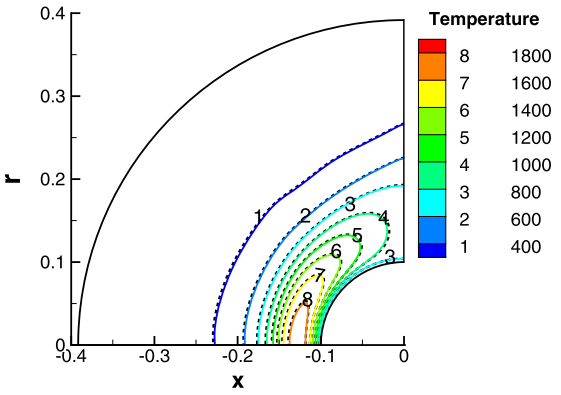


**Fig. 8.** Temperature contours for the flow past a half-sphere at Ma = 5 and Kn = 0.236. Solid lines: implicit UGKS-AS; dashed lines: explicit UGKS-AS.

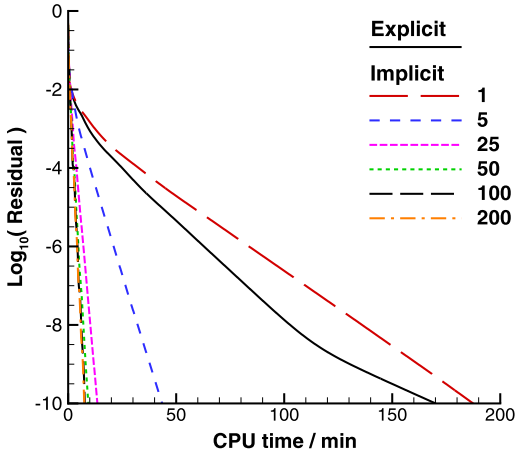


**Fig. 9.** Residuals of UGKS-AS under different $n_t$ for the flow past a half-sphere.

**Table 1**
Total steps, CPU time and acceleration rate of implicit UGKS-AS under different $n_t$ for the flow past a half-sphere at Ma = 5 and Kn = 0.236.

| $n_t$ | Explicit | 1 | 5 | 25 | 50 | 100 | 200 |
|---|---|---|---|---|---|---|---|
| Step | 5607 | 5001 | 1131 | 331 | 230 | 188 | 184 |
| CPU time (min) | 168.9 | 186 | 41.9 | 12.5 | 8.49 | 6.83 | 6.80 |
| Acceleration rate | 1 | 0.91 | 4.0 | 13.5 | 19.9 | 24.7 | 24.8 |

when $n_t$ approaches to 100. As a result, the efficiency of UGKS-AS is increased by more than one order of magnitude with the help of implicit technique in this case.

The density, pressure, and temperatures profiles along two typical lines predicted by implicit UGKS-AS, DVM [1], and the full 3D UGKS [32] are shown in Fig. 10, where $\bar{r}$ is the radial distance from the sphere center. The wall pressure, shear stress, and heat flux are presented in Fig. 11. The results of implicit UGKS-AS with refined grid points $(33, 27, 63)$ in $(u, \zeta, \omega)$ are also included in Fig. 10 and Fig. 11 to validate the grid convergence. It is encouraging to get such a good agreement by implicit UGKS-AS with other existing studies by such a low computational cost: 3000 grids in physical space, 2079 in velocity space, and 6.8 min of CPU time in total (about 184 steps). On the other hand, it will be rather difficult for a full 3D computation in hours of CPU time with cumbersome mesh generation near the singularity point and possible parallel implementation. Even using 3D unstructured mesh, the computational cost is still much larger and the axial symmetry can not be preserved similarly when solving axisymmetric flows.

More comparisons are made between the grid converged results from implicit UGKS-AS with the experiment measurements [33–39] for flow passing a sphere with a wide range of free stream Kn and Re under Ma = 2. The drag coefficient is defined as $C_D = F_D/(0.5\rho_\infty U_\infty^2 \pi r_s^2)$ where $F_D$ is the drag force. The stagnation heat transfer coefficient is calculated by $C_H = q_w/q_{FM}$, where $q_w$ is the stagnation heat transfer and $q_{FM}$ is the value in free molecular limit [40]. The hard sphere monatomic gas with Shakhov model [31] and Pr = 2/3 is simulated here. The wall surface temperature is equal to

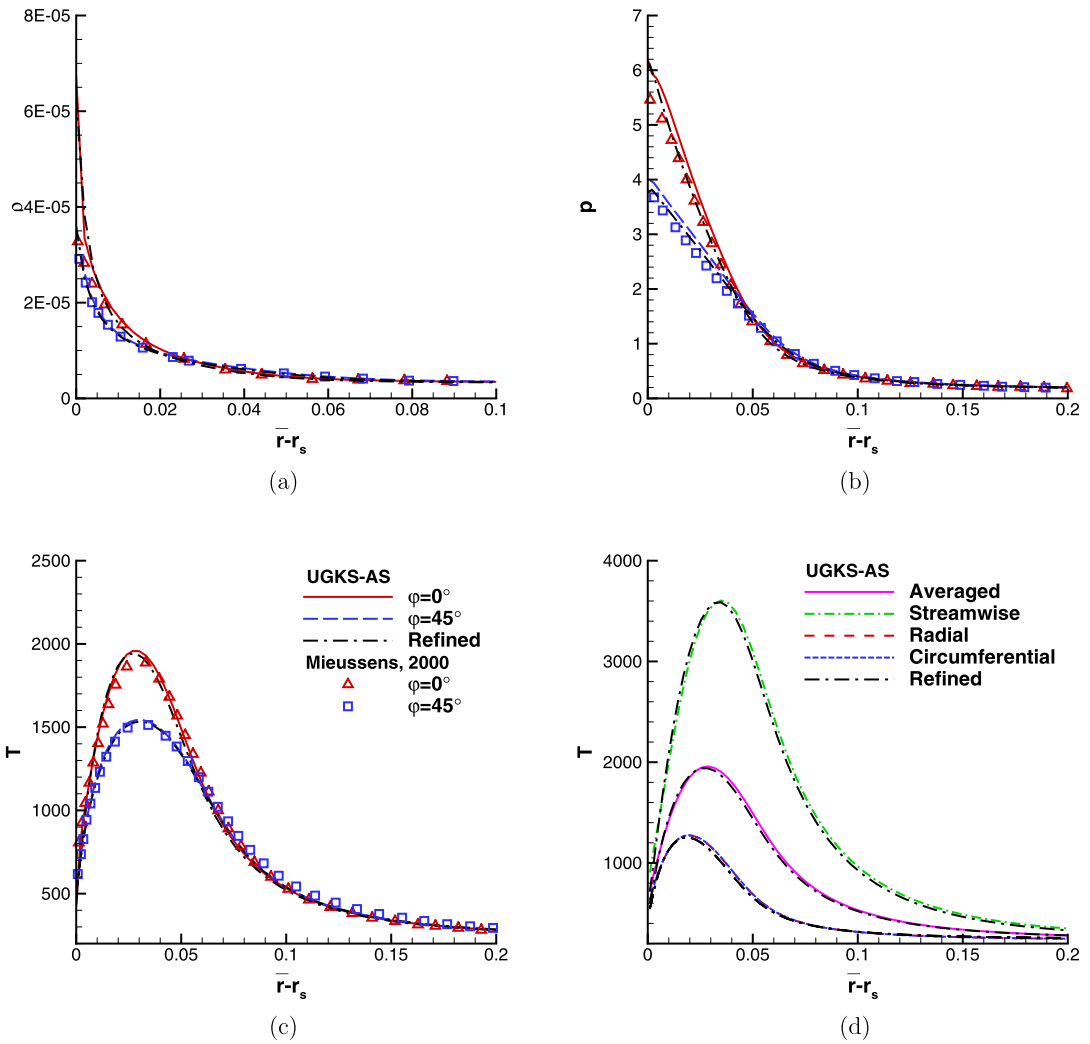


**Fig. 10.** (a) Density; (b) pressure; (c) averaged temperature along the symmetric axis ($\varphi = 0°$) and $\varphi = 45°$ from the symmetric axis for the flow past a half-sphere. Figure (d) is the temperatures in different directions along the symmetry axis.

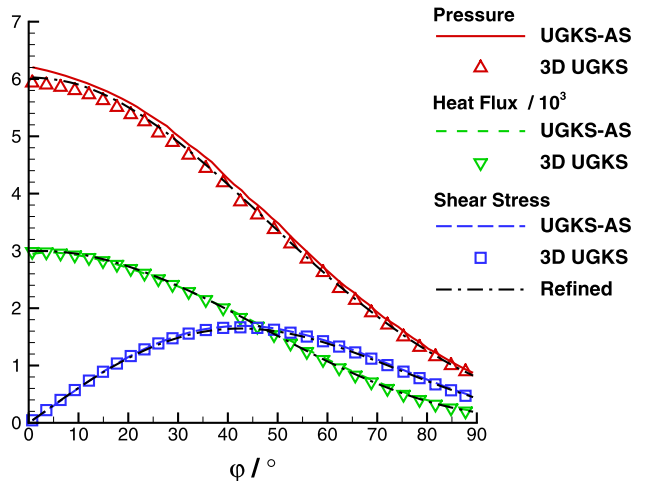


**Fig. 11.** Wall pressure, shear stress, and heat flux for the flow past a half-sphere at Ma = 5 and Kn = 0.236. Lines: implicit UGKS-AS; symbols: the full 3D UGKS [32].

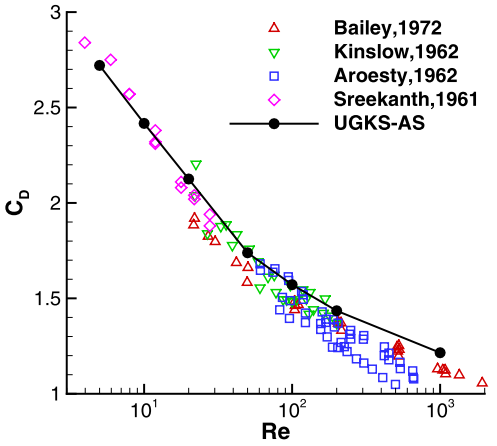


**Fig. 12.** Drag coefficient for the flow past a sphere.

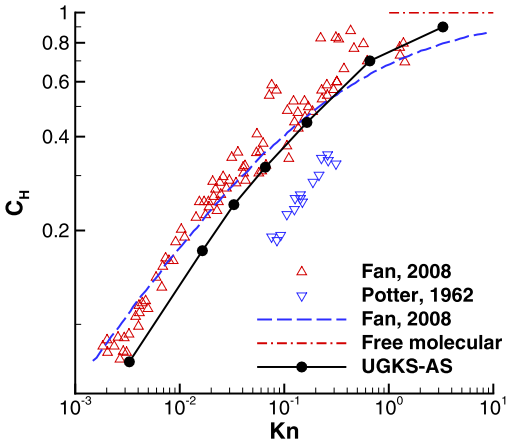


**Fig. 13.** Stagnation heat transfer coefficient for the flow past a half-sphere. Solid line: implicit UGKS-AS; symbols: experiment [38]; dashed lines: fitting curve of the experiments [37].

the upstream total temperature $T_0$ for $C_D$ and $0.123T_0$ for $C_H$ [41]. The predicted $C_D$ and $C_H$ by UGKS-AS are shown in Figs. 12 and 13, together with the results from experiments under different gas type, Mach number, et al. The trend over Re or Kn from UGKS-AS is in good agreement with the experiments. The quantitative results also provide a supplement to this practically interested problem. In Fig. 14 and Fig. 15, the flow fields under $\mathrm{Re} = 1000$, 100 and 10 are shown, corresponding to $\mathrm{Kn} = 0.0033$, 0.033 and 0.33, in which dramatic changes can be clearly observed, such as the shock structure and the leeward region flow. Once again, the present developed UGKS-AS shows good accuracy and efficiency in high-speed axisymmetric rarefied flow.

### 3.4. Force driven cylindrical Poiseuille flow

The force driven Poiseuille flow has been of great interest as a fundamental scientific problem. The Knudsen paradox, central minimum temperature, and the non-constant pressure along the transverse direction, are the striking features [42, 43]. The existing study includes the analytic methods with slip boundary conditions, semi-analytic methods for small driven force based on the linearized Boltzmann equation, or the simplified source term for near-continuum flows [2,44–50]. DSMC and other full 3D computations are also carried out in similar problems [43,27]. However, for cylindrical Poiseuille flow inside a pipe with circular section, there still lacks benchmark solutions over the transition regime with medium and large driven force. The meticulous results of this fundamental problem, like the small variations of temperature, pressure, and the distribution functions, are still few and far from a complete picture. It is rather difficult to resolve the force driven Poiseuille flow with high rarefaction and large driven force by a simulation with coarse velocity mesh. Even in the plane case, the highly distorted distribution functions can be hardly captured [31,46]. For the quasi-2D models, to keep the conservative property of the discrete source term is crucially important for the flow simulation around the symmetry axis [1]. Because of the high demand for a refined mesh in velocity space to resolve the small variation of flow fields, this problem is a

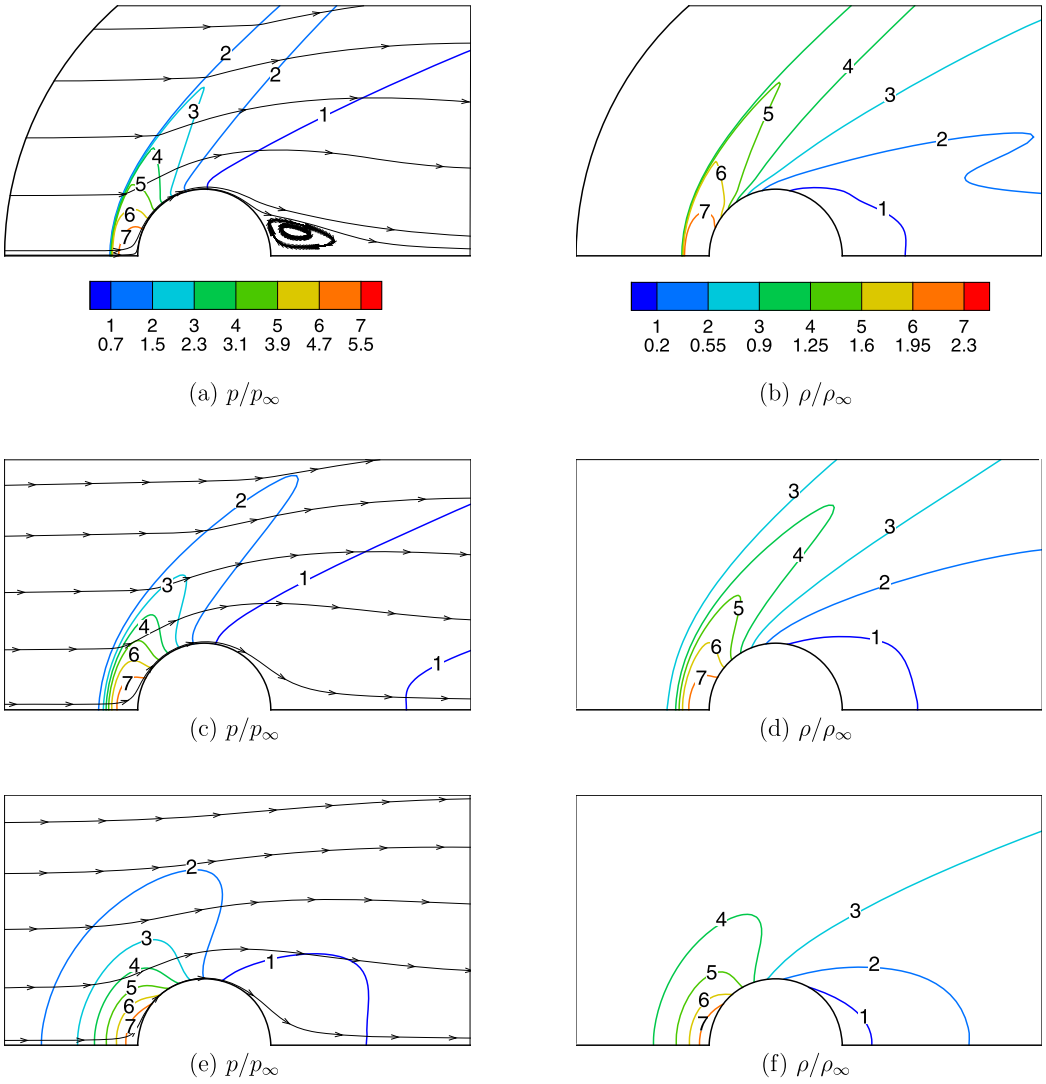


**Fig. 14.** Pressure, density contours and streamtraces for the flow past a sphere at Ma = 2, (a) and (b) Re = 1000; (c) and (d) Re = 100; (e) and (f) Re = 10.

challenging one even for the full 3D simulation. In the present study this flow is simulated by UGKS-AS over the transition regime with different intensities of driven force.

The hard sphere monatomic gas with Shakhov model [31] is simulated for Prandtl number $\Pr = 2/3$ and dimensionless gas constant $R = 1$. The difference from various collision models is not considered here. For better analysis, the reference variables are chosen as length $L_{ref} = 2r_s$ where $r_s = 0.5$ is the pipe radius, velocity $U_{ref} = \sqrt{RT_w}$, along with the average density $\rho_{av}$ and wall temperature $T_w$. The Knudsen number $\mathrm{Kn} = \lambda/r_s$ is defined based on $\rho_{av}$ and $T_w$. The pipe wall is diffusive and isothermal with constant temperature $T_w = 1$. The driven force $\rho\hat{a}$ is nondimensionalized as $G = \rho\hat{a}/\left(\rho_{av}U_{ref}^2/L_{ref}\right)$. The corresponding induced velocity and the temperature increase are positively correlated with $G/\mathrm{Kn}$, which can be used to qualitatively evaluate the deviation from isothermal flow.

As the wall slip and the distortion of distribution function become significant when the rarefaction effect increases, for a grid convergent solution, refined velocity mesh points are adopted: $(81, 81, 120)$ in $(u, \zeta, \omega)$ for $\mathrm{Kn} \le 5$, $(121, 101, 200)$ for $5 < \mathrm{Kn} \le 10$, and $(121, 121, 240)$ for $\mathrm{Kn} > 10$, with $\alpha_{umax} = 10, \alpha_{umin} = 7, \alpha_{\zeta max} = 7$. Here $r$ in $[0, 0.5]$ is divided uniformly into 20 cells. The CFL number is set to be 0.6.

The driven force $\rho\hat{a}$ is included as an acceleration source term $\hat{a}\partial f/\partial u$ on the left side of Eq. (20). The particle velocity $u_l$ in $g$ and $f_0$ in the analytical solution Eq. (4) is changed to $u_l - \hat{a}t$. The force accelerates the particle movement and deviates the characteristic line from its original direction by $\hat{a}\Delta t$ in each time step. For all cases in this section, the acceleration effect satisfies the condition $\hat{a}\Delta t < 10^{-3}U_{ref} \ll 0.1U_{ref} < \Delta u$. The characteristic line almost keeps along its original direction in $\Delta t$. The time scale due to the acceleration source term, i.e., $\Delta u/\hat{a}$, is much larger than the time step. As a result, the acceleration effect seems frozen. Numerically, when the acceleration term $(0, -1, 0, 0, -U)^{\mathrm{T}}\rho\hat{a}\Delta t$ and $\hat{a}\Delta t\partial f/\partial u$ are

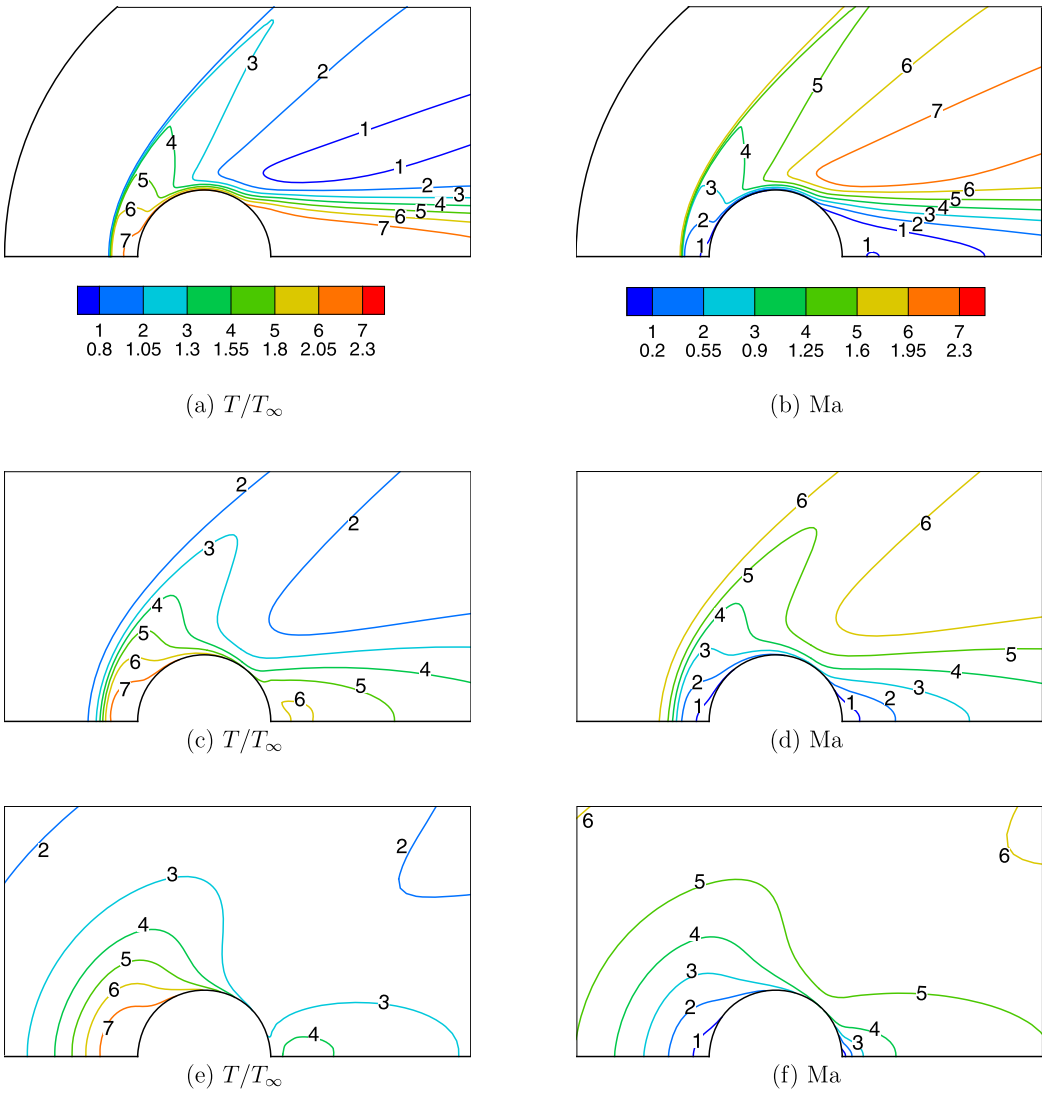


**Fig. 15.** Temperature, Ma contours for the flow past a sphere at Ma = 2, (a) and (b) Re = 1000; (c) and (d) Re = 100; (e) and (f) Re = 10.

added to update **W** and $f$ with first-order accuracy in time, there's no necessary for considering the acceleration effect when constructing the time evolution of distribution function as the acceleration effect is second-order in time in the flux evaluation. Central difference in $u$ is used to construct $\partial f/\partial u$.

Firstly, $\mathrm{Kn} = 0.32/\pi, 0.64/\pi, 6.4/\pi$ with $G = 1$ are simulated and compared with the plane flow [31]. For this case, the conservation properties are crucial. In order to get the small variations in temperature and pressure, the explicit UGKS-AS is applied. The predicted density, velocity, and pressure profiles are shown in Fig. 16. It is not surprising that the maximum velocity in the axisymmetric case is smaller than that in the plane case [31]. The non-constant pressure profile is observed in the axisymmetric case. The temperature profiles are shown in Fig. 17, and the streamwise temperature diverges from the radial and circumferential ones. Different from the plane flow, the temperature difference between the radial and the circumferential one in the axisymmetric case is much less, which shows the similar effect from the constraint of the circular wall on the particle velocity in these two directions. The averaged temperature shows a central minimum even at small Knudsen number $\mathrm{Kn} = 0.32/\pi$, and the streamwise temperature has a clear ring peak structure which is similar to the plane case. For $\mathrm{Kn} = 6.4/\pi$, the averaged temperature and streamwise temperature still show a central minimum although the radial and circumferential temperatures decrease from the tube center to the solid wall. These quantitative results of the cylindrical Poiseuille flow provide a new benchmark solution for micro flow study.

The cylindrical Poiseuille flows in a wider range of Knudsen numbers, i.e., $1.6/\pi \le \mathrm{Kn} \le 38.4/\pi$, are then simulated with explicit UGKS-AS. The corresponding $G$ is 0.2 for $\mathrm{Kn} = 1.6/\pi$, 0.3 for $\mathrm{Kn} = 3.2/\pi, 6.4/\pi$, and 0.4 else. The driven force preserves the maximum $\mathrm{Ma} < 0.3$ as $G/\mathrm{Kn}$ is not large. The velocity, pressure, and temperature profiles for Kn =

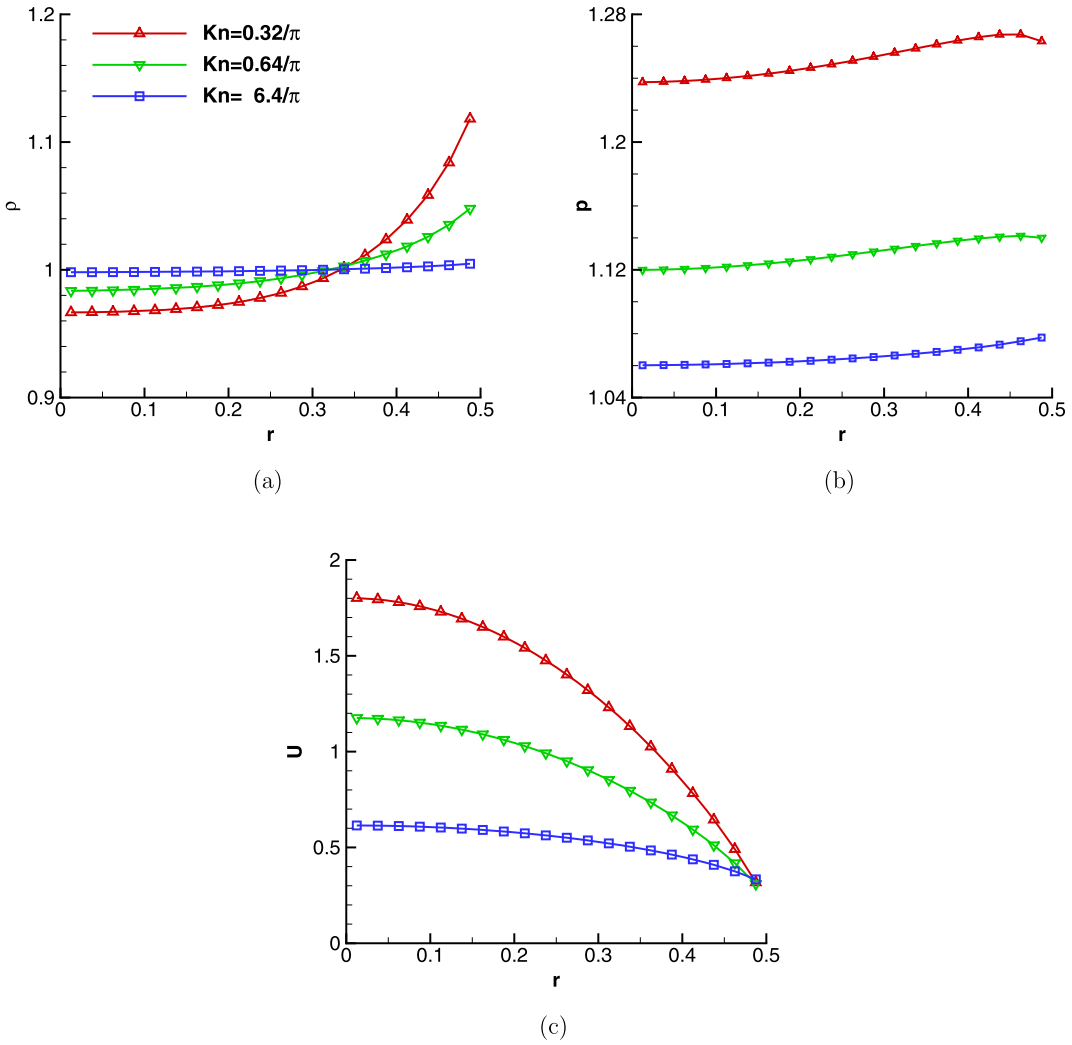


**Fig. 16.** (a) Density; (b) pressure; (c) axial velocity for force driven cylindrical Poiseuille flow at different Kn.

$12.8/\pi, 25.6/\pi, 38.4/\pi$ with $G = 0.4$ are shown in Fig. 18, which are similar to the above-mentioned results for $\mathrm{Kn} = 6.4/\pi$ and $G = 1$. Due to the small $G/\mathrm{Kn}$, the temperature increase is less than 3%. Thus, the results from the linearized kinetic equations can be compared, in which the flow is considered to be isothermal [51,48,47]. The calculated mass flow rate normalized by the free molecular result [45] is shown in Fig. 19. The UGKS-AS captures the Knudsen paradox successfully, which illustrates the high accuracy of UGKS-AS for the cases with small variation of flow field.

The distribution functions near the center of the pipe at $v_\theta$ approaching 0 $(j = 1, q = 1)$ are also shown in Fig. 20. Under the three large Knudsen numbers, i.e., $\mathrm{Kn} = 12.8/\pi, 25.6/\pi, 38.4/\pi$, the distribution functions are highly distorted from Maxwellian equilibrium into a double-peak structure. To get accurate solutions, not only $U$, but also temperature and pressure, the double peaks and the slopes between them have to be well resolved. In fact, the distorted part is mainly located within a small $\Delta v_r$ region. As rarefaction effect becomes larger, the distorted slopes become much steeper. That's why the refined velocity mesh points are required in the force driven case, especially for $\mathrm{Kn} \geq 1$. The narrow distorted distribution function in this case is similar to that in the pressure driven planar channel flow found by Ohwada [46] based on the linearized method. The linearized method is valid under the following constraints. The distribution function is supposed to be not far away from equilibrium; $G$ is very small; and the temperature variations are very small as well [48,46]. For the force driven case considered in this study, the distribution function is highly distorted, and has more complicated structures, especially at high Kn. The present results given by UGKS-AS are reliable and provide a complement one from previous solutions. For the force driven cylindrical Poiseuille flow, it is still a challenge for a full 3D accurate solution with affordable computational cost.

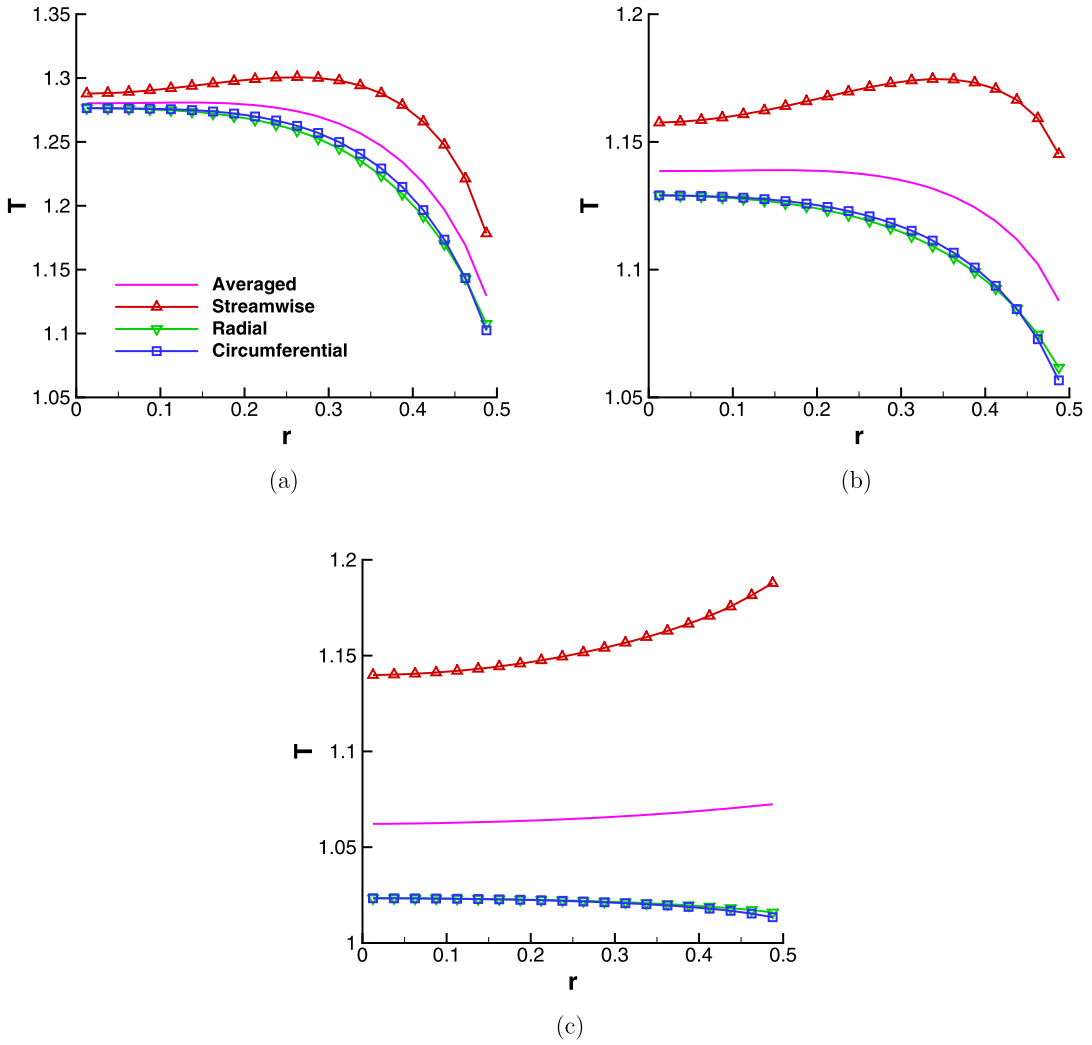


**Fig. 17.** Averaged temperature and the temperatures in the streamwise, radial, and circumferential directions for force driven cylindrical Poiseuille flow at (a) $\mathrm{Kn} = 0.32/\pi$; (b) $\mathrm{Kn} = 0.64/\pi$; (c) $\mathrm{Kn} = 6.4/\pi$.

## 4. Conclusions

In this paper, a unified gas-kinetic scheme for axisymmetric flow, the so called UGKS-AS, has been developed based on the axisymmetric quasi-2D model equation. Based on the coordinate transformation between the local Cartesian and cylindrical coordinates, the source term as well as the flux transport across cell interface in the axisymmetric model is evaluated with the help of the time evolution solution of the full 3D BGK equation in the local Cartesian coordinates. The particle free transport and collision are coupled in the flux and source term evaluation. The explicit UGKS-AS is developed for both non-conservative and conservative formulations for the axisymmetric flow. At the same time, an implicit UGKS-AS is proposed for the updates of both macroscopic flow variables and microscopic distribution function. In comparison with the full 3D scheme, the UGKS-AS has the following advantages. Firstly, the computational cost is much reduced due to the absence of circumferential coordinate discretization. Secondly, the scheme can present accurate NS solutions in the continuum regime without imposing the time step being less than the particle collision time. Thirdly, it provides accurate solutions in the whole flow regimes with high efficiency, especially for the implicit scheme.

Typical axisymmetric flows are simulated by the current UGKS-AS, including the internal flow between coaxial cylinders, external flow passing through a sphere, and the force driven cylindrical Poiseuille flow from continuum to the free molecular regime. The time step for the explicit UGKS-AS is determined by the CFL condition, which reveals the high efficiency by UGKS-AS in the unsteady and multiple scale axisymmetric flow applications. With the introduction of the trigonometric operators, the UGKS-AS is capable of giving accurate results on a very low grid resolution in typical axisymmetric flow, such as the internal flow or external flow with high speeds, where the full 3D model can be hardly used under limited resources. With the implicit implementation, the efficiency of UGKS-AS can be improved by one order of magnitude in comparison

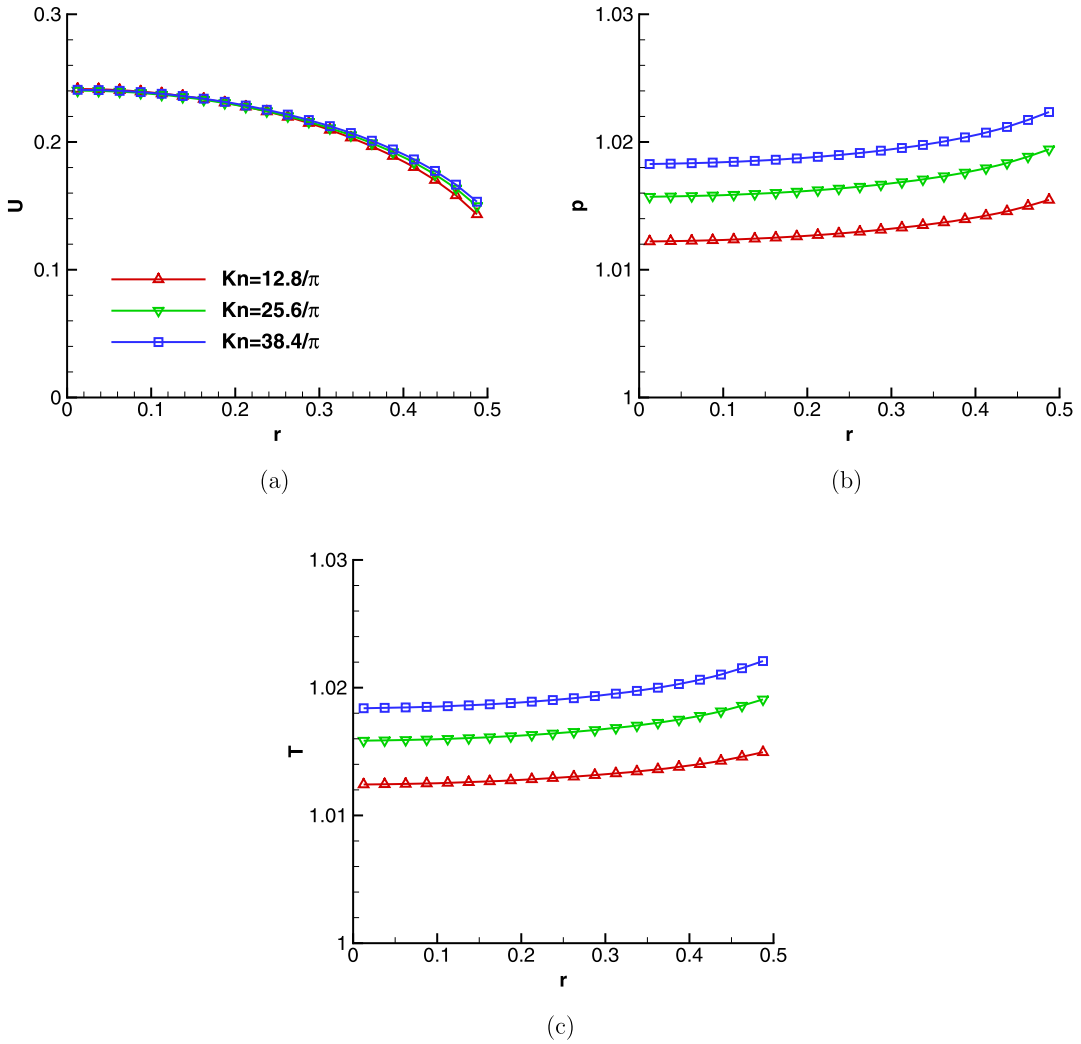


**Fig. 18.** (a) Axial velocity; (b) pressure; (c) averaged temperature profile for force driven cylindrical Poiseuille flow at different Kn.

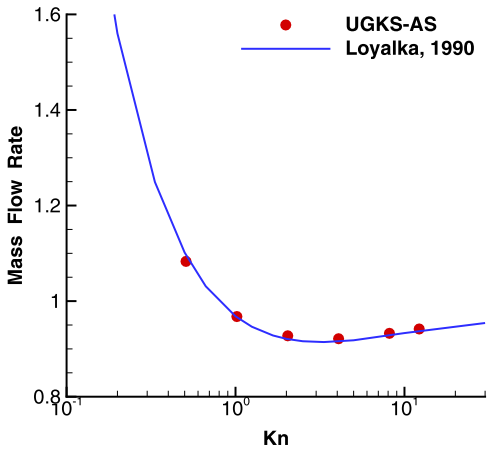


**Fig. 19.** Mass flow rate normalized by the free molecular result [45] for force driven cylindrical Poiseuille flow. Line: the corresponding BGK model results in [47].

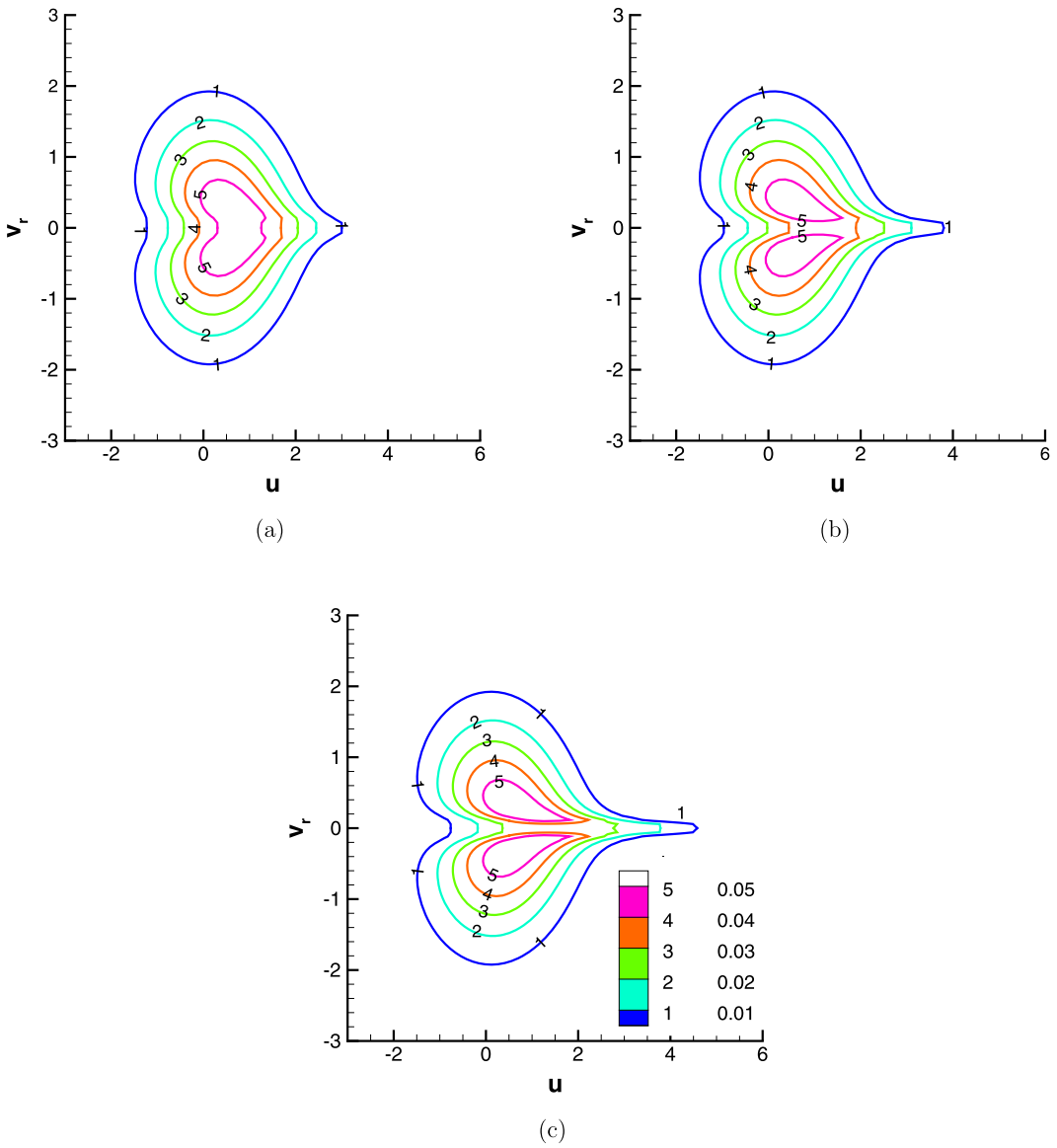


**Fig. 20.** Distribution function for force driven cylindrical Poiseuille flow at (a) $\mathrm{Kn} = 12.8/\pi$; (b) $\mathrm{Kn} = 25.6/\pi$; (c) $\mathrm{Kn} = 38.4/\pi$.

with the explicit scheme. In the cylindrical Poiseuille flow, near symmetry axis a highly distorted distribution functions and small variation of macroscopic quantities have been captured. The UGKS-AS not only presents accurate integral solution, such as the mass flux across the tube, but also gives reliable temperature profiles and distribution functions. The cylindrical Poiseuille flow solutions provided by UGKS-AS can be used as benchmark solutions.

In this work the quasi-2D model for axisymmetric flow is solved under the UGKS framework. The techniques developed in this paper can be easily extended to solve other axisymmetric transport equations, such as the radiative transfer and plasma physics [52,53]. The success for UGKS is the closed coupling of the particle transport, collision, and other possible source term, such as gravity, in the evaluation of the time evolution gas distribution function for the flux evaluation. In the future, more complicated transport process, such as turbulence and multi-phase flow will be studied under the direction modeling methodology of UGKS [54].

## Acknowledgements

This work is supported by the National Key Basic Research and Development Program (2014CB744100), National Natural Science Foundation of China (91330203, 11172154, 91530319), Science Challenge Project (TZ2016001) and Special Program for Applied Research on Super Computation of the NSFC-Guangdong Joint Fund (the second phase) (U1501501). We also

would like to acknowledge the technical support of PARATERA and the “Explorer 100” cluster system of Tsinghua National Laboratory for Information Science and Technology.

## References

[1] L. Mieussens, Discrete-velocity models and numerical schemes for the Boltzmann-BGK equation in plane and axisymmetric geometries, J. Comput. Phys. 162 (2000) 429–466.
[2] Z.L. Guo, H.F. Han, B.C. Shi, C.G. Zheng, Theory of the lattice Boltzmann equation: lattice Boltzmann model for axisymmetric flows, Phys. Rev. E 79 (2009) 046708.
[3] P.B. Yu, A Unified Gas Kinetic Scheme for All Knudsen Number Flows, Ph.D. thesis, The Hong Kong University of Science and Technology, 2013.
[4] L. Zhu, Z. Guo, K. Xu, Discrete unified gas kinetic scheme on unstructured meshes, Comput. Fluids 127 (2016) 211–225.
[5] K. Aoki, H. Yoshida, T. Nakanishi, A.L. Garcia, Inverted velocity profile in the cylindrical Couette flow of a rarefied gas, Phys. Rev. E 68 (2003) 016302.
[6] D. Bergers, Kinetic model solution for axisymmetric flow by the method of discrete ordinates, J. Comput. Phys. 57 (1985) 285–302.
[7] G.H. Zhang, S. Fu, J.B. Zhao, BGK-equation simulation of the exhaust plume formed by a manoeuvre thruster in outer space, Acta Mech. Sin. 17 (2001) 225–236.
[8] Y. Sone, S. Takata, H. Sugimoto, The behavior of a gas in the continuum limit in the light of kinetic theory: the case of cylindrical Couette flows with evaporation and condensation, Phys. Fluids 8 (1996) 3403–3413.
[9] Y. Sone, H. Sugimoto, K. Aoki, Cylindrical Couette flows of a rarefied gas with evaporation and condensation: reversal and bifurcation of flows, Phys. Fluids 11 (1999) 476–490.
[10] H. Sugimoto, Y. Sone, Numerical analysis of steady flows of a gas evaporating from its cylindrical condensed phase on the basis of kinetic theory, Phys. Fluids 4 (1992) 419–440.
[11] G.A. Bird, Breakdown of translational and rotational equilibrium in gaseous expansions, AIAA J. 8 (1970) 1998–2003.
[12] X.Y. He, X.W. Shan, G.D. Doolen, Discrete Boltzmann equation model for nonideal gases, Phys. Rev. 57 (1998) R13–R16.
[13] K. Xu, A gas-kinetic BGK scheme for the Navier–Stokes equations and its connection with artificial dissipation and Godunov method, J. Comput. Phys. 171 (2001) 289–335.
[14] Q.B. Li, S. Fu, K. Xu, Application of gas-kinetic scheme with kinetic boundary conditions in hypersonic flow, AIAA J. 43 (2005) 2170–2176.
[15] K. Xu, J.C. Huang, A unified gas-kinetic scheme for continuum and rarefied flows, J. Comput. Phys. 229 (2010) 7747–7764.
[16] J.C. Huang, K. Xu, P.B. Yu, A unified gas-kinetic scheme for continuum and rarefied flows II: multi-dimensional cases, Commun. Comput. Phys. 12 (2012) 662–690.
[17] J.C. Huang, K. Xu, P.B. Yu, A unified gas-kinetic scheme for continuum and rarefied flows III: microflow simulations, Commun. Comput. Phys. 14 (2013) 1147–1173.
[18] M. Bennoune, M. Lemou, L. Mieussens, Uniformly stable numerical schemes for the Boltzmann equation preserving the compressible Navier–Stokes asymptotics, J. Comput. Phys. 227 (2008) 3781–3803.
[19] S. Jin, Asymptotic preserving (AP) schemes for multiscale kinetic and hyperbolic equations: a review, Riv. Mat. Univ. Parma 2 (2010) 177–216.
[20] S.Z. Chen, K. Xu, A comparative study of an asymptotic preserving scheme and unified gas-kinetic scheme in continuum flow limit, J. Comput. Phys. 288 (2015) 52–65.
[21] M.L. Mao, D.W. Jiang, J. Li, X.G. Deng, Study on implicit implementation of the unified gas kinetic scheme, Chin. J. Theoret. Appl. Mech. 47 (2015) 822–829.
[22] Y.J. Zhu, C.W. Zhong, K. Xu, Implicit unified gas-kinetic scheme for steady state solutions in all flow regimes, J. Comput. Phys. 315 (2016) 16–38.
[23] Q.B. Li, S. Fu, Applications of implicit BGK scheme in near-continuum flow, J. Comput. Phys. 20 (2006) 453–461.
[24] D.W. Jiang, M.L. Mao, J. Li, X.G. Deng, Study on the numerical error introduced by dissatisfying the conservation constraint in UGKS and its effects, Chin. J. Theoret. Appl. Mech. 47 (2015) 163–168.
[25] V. Titarev, M. Dumbser, S. Utyuzhnikov, Construction and comparison of parallel implicit kinetic solvers in three spatial dimensions, J. Comput. Phys. 256 (2014) 17–33.
[26] S.Y. Li, Q.B. Li, S. Fu, A unified gas-kinetic scheme for axisymmetric flow, in: J. Fan (Ed.), Proceedings of the 29th International Symposium on Rarefied Gas Dynamics, vol. 1628, AIP Publishing, 2014, pp. 976–979.
[27] V.A. Titarev, E.M. Shakhov, S.V. Utyuzhnikov, Rarefied gas flow through a diverging conical pipe into vacuum, Vacuum 101 (2014) 10–17.
[28] P. Gospodinov, V. Roussinov, D. Dankov, Thermoacoustic waves in a cylindrical Couette rarefied gas flow, in: M.D. Todorov (Ed.), 6th International Conference for Promoting the Application of Mathematics in Technical and Natural Sciences, vol. 1629, AIP Publishing, 2014, pp. 296–302.
[29] P. Gospodinov, D. Dankov, V. Roussinov, Thermo acoustic waves in rarefied gas between two coaxial cylinders at a sudden change of the temperature of the outer cylinder, in: M.D. Todorov (Ed.), 8th International Conference for Promoting the Application of Mathematics in Technical and Natural Sciences, vol. 1773, AIP Publishing, 2016, 080001.
[30] I. Graur, M.T. Ho, M. Wuest, Simulation of the transient heat transfer between two coaxial cylinders, J. Vac. Sci. Technol. A 31 (2013) 061603.
[31] S.Z. Chen, K. Xu, Q.D. Cai, A comparison and unification of ellipsoidal statistical and Shakhov BGK models, Adv. Appl. Math. Mech. 7 (2015) 245–266.
[32] S.Y. Li, Q.B. Li, S. Fu, J.X. Xu, The high performance parallel algorithm for unified gas-kinetic scheme, in: A. Ketsdever, H. Struchtrup (Eds.), Proceedings of the 30th International Symposium on Rarefied Gas Dynamics, vol. 1786, AIP Publishing, 2016, 180007.
[33] A.B. Bailey, J. Hiatt, Sphere drag coefficients for a broad range of Mach and Reynolds numbers, AIAA J. 10 (1972) 1436–1440.
[34] M. Kinslow, J.L. Potter, The Drag of Spheres in Rarefied Hypervelocity Flow, Tech. Rep. AEDC-TDR-62-205, ARO, Inc., Dec. 1962.
[35] J. Aroesty, Sphere Drag in a Low-Density Supersonic Flow, Tech. Rep. HE-150-192, University of California, Jan. 1962.
[36] A.K. Sreekanth, Drag Measurements on Circular Cylinders and Spheres in the Transition Regime at a Mach Number of 2, Tech. Rep. UTIA Report no. 74, University of Toronto, Apr. 1961.
[37] J. Fan, J.Z. Jiang, C.X. Wu, Rarefied gas effects on stagnation heat flux of hypersonic flows, in: Proceedings of the 1st Symposium on Hypersonic Science and Technology, 2008, pp. CSTAM–2008–0003:1–3.
[38] S.C. Metcalf, G.T. Coleman, C. Berry, Heat transfer to bluff and hemispherical faced cylinders between continuum and free molecular limits, in: B. Manfred, F. Martin (Eds.), Proceedings of the 9th International Symposium on Rarefied Gas Dynamics, vol. 2, AIP Publishing, 1974, pp. D16:1–11.
[39] J.L. Potter, J.T. Miller, Total heating load on blunt axisymmetric bodies in low-density flow, AIAA J. 1 (1963) 480–481.
[40] Q. Shen, Rarefied Gas Dynamics, National Defence Industry Press, 2003 (in Chinese).
[41] J.L. Potter, J.T. Miller, Experimental Heat Transfer to Blunt Axisymmetric Bodies Near the Limit of Continuum Flow, Tech. Rep. AEDC-TDR-62-155, ARO, Inc., Aug. 1962.
[42] T. Kanki, S. Iuchi, Poiseuille flow and thermal creep of a rarefied gas between parallel plates, Phys. Fluids 16 (1973) 594–599.
[43] Y.H. Zheng, A.L. Garcia, B.J. Alder, Comparison of kinetic theory and hydrodynamics for Poiseuille flow, J. Stat. Phys. 109 (2002) 495–505.
[44] H.W. Liu, Gas-Kinetic Methods for Viscous Fluid Flows, Ph.D. thesis, The Hong Kong University of Science and Technology, 2007.
[45] A. Beskok, G.E. Karniadakis, Report: a model for flows in channels, pipes, and ducts at micro and nano scales, Microscale Thermophys. Eng. 3 (1999) 43–77.

[46] T. Ohwada, Y. Sone, K. Aoki, Numerical analysis of the Poiseuille and thermal transpiration flows between two parallel plates on the basis of the Boltzmann equation for hard-sphere molecules, Phys. Fluids 1 (1989) 2042–2049.
[47] S.K. Loyalka, S.A. Hamoodi, Poiseuille flow of a rarefied gas in a cylindrical tube: solution of linearized Boltzmann equation, Phys. Fluids 2 (1990) 2061–2065.
[48] V.A. Titarev, Rarefied gas flow in a circular pipe of finite length, Vacuum 94 (2013) 92–103.
[49] L. Wu, J. Zhang, H.H. Liu, Y.H. Zhang, J.M. Reese, A fast iterative scheme for the linearized Boltzmann equation, J. Comput. Phys. 338 (2017) 431–451.
[50] L. Wu, H. Struchtrup, Assessment and development of the gas kinetic boundary condition for the Boltzmann equation, J. Fluid Mech. 823 (2017) 511–537.
[51] F. Sharipov, V. Seleznev, Data on internal rarefied gas flows, J. Phys. Chem. Ref. Data 27 (1998) 657–706.
[52] W.J. Sun, S. Jiang, K. Xu, An implicit unified gas kinetic scheme for radiative transfer with equilibrium and non-equilibrium diffusive limits, Commun. Comput. Phys. 22 (2017) 889–912.
[53] C. Liu, K. Xu, A unified gas kinetic scheme for continuum and rarefied flows V: multiscale and multi-component plasma transport, Commun. Comput. Phys. 22 (2017) 1175–1223.
[54] K. Xu, C. Liu, A paradigm for modeling and computation of gas dynamics, Phys. Fluids 29 (2017) 026101.